



Biogeochemical fluxes and fate of diazotroph derived nitrogen in the food web after a phosphate enrichment: Modeling of the VAHINE mesocosms experiment

Audrey Gimenez¹, Melika Baklouti¹, Sophie Bonnet^{1,2}, and Thierry Moutin¹

¹ Aix Marseille Université, CNRS/INSU, Université de Toulon, IRD, Mediterranean Institute of Oceanography (MIO) UM110, 13288, Marseille, France

² Institut de Recherche pour le Développement (IRD), AMU/CNRS/INSU, Université de Toulon, Mediterranean Institute of Oceanography (MIO) UM 110, 13288, Noumea, France-New Caledonia

Correspondence to: A. Gimenez (audrey.gimenez@mio.osupytheas.fr)

Abstract. The VAHINE mesocosm experiment in the oligotrophic waters of the Noumea lagoon (New Caledonia) aimed to assess the role of the nitrogen input through N₂ fixation on carbon production and export, and to study the fate of diazotroph-derived nitrogen (DDN) throughout the planktonic food web. A 1D-vertical biogeochemical mechanistic model was used in addition to the *in situ* experiment to complement our comprehension of the dynamics of the planktonic ecosystem and the main biogeochemical carbon (C), nitrogen (N), phosphate (P) fluxes. The mesocosms were intentionally enriched with 0.8 μmol.L⁻¹ of P to trigger the development of diazotrophs and amplify biogeochemical fluxes. Two simulations were run, one with and the other without the phosphate enrichment. In the P-enriched simulation, N₂ fixation, primary production and C export increased by 201, 208 and 87 %, respectively, consistent with the observed trends observed in the mesocosms (+ 124 %, + 141 %, + 261 % for N₂ fixation, PP and C export, respectively). The increase in primary and export productions became significant 10 days after the DIP enrichment, indicating that i) several days were necessary to obtain a significant response at the population scale, and ii) classical methods (short-term microcosms experiments) used to quantify nutrient limitations of primary production may not be relevant. The model allowed to follow the fate of fixed N₂ by providing over time the proportion of DDN in each compartment (mineral and organic) of the model. At the end of the simulation (25 days), 43 % of the DDN was found in the non-diazotroph organisms, 33 % in diazotrophs, 16 % in the dissolved organic nitrogen pool, 3 % in the particulate detrital organic pool and 5 % in traps, indicating that N₂ fixation efficiently benefitted to non-diazotrophic organisms and contributed to C export.



1 Introduction

Dinitrogen (N_2) fixation is the major external source of new nitrogen (N) for the upper ocean (Gruber and Galloway, 2008; Mahaffey et al., 2005) and particularly in the south-western Pacific ocean (Raimbault and Garcia, 2008; Moutin et al., 2008), which is recognized as one of the highest N_2 fixation area in the global ocean (Luo et al., 2012; Bonnet et al., 2015). While N availability primarily controls autotrophic plankton growth in low nutrient low chlorophyll (LNLC) ecosystems (Moore et al., 2001a; Graziano et al., 1996), the new N sources provided by N_2 fixation may drive the planktonic ecosystem from N limitation toward P limitation and may potentially affect the magnitude of C fixation, and eventually C export through the so called N_2 -primed prokaryotic C pump (Karl et al., 2003, 2012). Consequently, it is important to quantify N fluxes to the ocean as well as to study the fate of N newly fixed by diazotrophs (or diazotroph-derived N, hereafter referred to as DDN) to understand how N_2 fixation affects nutrient cycles and productivity in the ocean.

Biogeochemical models including N_2 fixation have been developed over the last decades, but only a few of them have included diazotrophic organisms as state variables (Rabouille et al., 2006). In these models, *Trichodesmium* is the most represented organism since it is the most studied diazotroph and its physiology is well documented in the literature (Moore et al., 2001b; Fennel et al., 2001; Moore et al., 2004; Rabouille et al., 2006). In recent studies, other diazotrophs such as unicellular Cyanobacteria (termed UCYN) or diatom-diazotroph associations (termed DDA) have been implemented in biogeochemical models. This was first done by Goebel et al. (2007) who developed a diagnostic model to assess the relative contribution of three distinct diazotrophs (i.e. *Trichodesmium* sp. and two UCYN from Group A and Group B (UCYN-A and UCYN-B, respectively) at the tropical North Pacific station ALOHA. More recently, other biogeochemical models including a more complex planktonic food web and the contribution of *Trichodesmium* sp., UCYN-A and UCYN-B were developed (Monteiro et al., 2010, 2011), together with models representing *Trichodesmium* sp., and a general group of UCYN (Dutkiewicz et al., 2012). Although more and more models include diazotrophic organisms as part of the food web, none of them have yet focused on the fate of DDN throughout the ecosystem. Diazotrophs release a part of the recently fixed N_2 as dissolved organic N (DON) and ammonium (NH_4^+) in the dissolved pool (Glibert and Bronk, 1994; Mulholland et al., 2006). The magnitude of this release (10 to 80 %) is still under debate in the scientific community (Glibert and Bronk, 1994; Konno et al., 2010; Benavides et al., 2013b, a) and seems to depend on the physiological state of the cells (Berthelot et al., 2015a) as well as on exogenous factors such as viral lysis (Hewson et al., 2004) or sloppy feeding (O'Neil et al., 1996). Nevertheless, recent methods coupling $^{15}N_2$ isotopic labeling, cell sorting by flow cytometry and high-resolution nanometer scale secondary ion mass spectrometry (nanoSIMS) analyses recently allowed to quantify the DDN transfer from diazotrophs to specific groups of non-diazotrophic phytoplankton and bacteria, indicating that the DDN released in the dissolved pool is available and actively used by surrounding non-diazotrophic communities (Bonnet et al. (a),subm., this issue).



The VAHINE project aimed to investigate the fate of DDN in oligotrophic ecosystems by deploying large-volume (50 m^3) mesocosms to isolate a water mass affected by a diazotroph development, and by combining both field biogeochemical/diversity measurements and a mechanistic modeling approach. The New Caledonian (Noumea) lagoon is considered as an oligotrophic ecosystem influenced by oceanic waters inflowing from outside the lagoon (Ouillon et al., 2010). It supports high N_2 fixation rates ($235 \mu\text{molN.m}^{-2}.\text{d}^{-1}$, Garcia et al. (2007)), high *Trichodesmium* sp. (Dupouy et al., 2000; Rodier and Le Borgne, 2008, 2010) and UCYN abundances (Biegala and Raimbault, 2008). This site therefore represented an ideal location to investigate the fate of DDN.

The mesocosms were intentionally enriched with dissolved inorganic phosphate (DIP) to enhance the potential development of N_2 fixers in the mesocosms, and therefore amplify N_2 fixation fluxes and facilitate the study of DDN pathways in the planktonic ecosystem. Complementary field approaches were used during the VAHINE project including a $\delta^{15}\text{N}$ budget to assess the dominant source of N (from NO_3^- - and/or N_2 fixation) fueling export production along the experiment (Knapp et al., subm., this issue). Bonnet et al. (a) (subm., this issue) explored the fate of DDN at shorter time scales, investigating the relative contribution of each diazotroph phylotype to direct C export, and quantifying the DDN release and its subsequent transfer to different groups of plankton by using nanoSIMS. In the present study, we developed a 1D-vertical biogeochemical model including the representation of *Trichodesmium* and UCYN diazotrophs of the Group C (UCYN-C, which developed extensively during the mesocosm experiment, (Turk-Kubo et al., subm., this issue)). The goal of this study was to complement our comprehension of the dynamics of the planktonic food web and the associated biogeochemical fluxes during the mesocosm experiment by providing information that could not be inferred through *in situ* measurements. We also used the model to follow the route of DDN into the different compartments of the ecosystem (diazotrophs, non-diazotrophs, dissolved pool, detrital pool and export).

2 Methods

2.1 The VAHINE experiment

The VAHINE experiment took place in January-February 2013 (austral summer) in the oligotrophic New Caledonian lagoon. Three large volume ($\sim 50 \text{ m}^3$, 15 m-height) mesocosms equipped with sediment traps fixed at their bottom were deployed and the dynamics of the three mesocosms was followed for 23 days. The full description of the mesocosms design and deployment, including selection of the study site and logistics are detailed in Bonnet et al. (b) (subm., this issue). The mesocosms were enriched with $\sim 0.8 \mu\text{mol.L}^{-1}$ of orthophosphate (PO_4^{3-}) on the evening of day 4 to alleviate any potential DIP limitation which is a constant feature observed in the south-western Pacific (Moutin et al., 2005, 2008) and stimulate N_2 fixation. Seawater was sampled daily in the three mesocosms (hereafter called M1, M2 and M3) and outside (hereafter called lagoon waters) at



three depths (1m, 6m and 12m) and the sediment traps were collected every 24 h by scuba divers. The methods used to measure the different variables (C, N, P pools and fluxes, chlorophyll a stocks and plankton abundances) used in the present paper for comparison with the model simulations are detailed in the companion papers of Berthelot et al. (2015b), Leblanc et al., subm., Van Wambeke et al., subm., this issue).

2.2 Mesocosm modeling and hypothesis

The model used in the VAHINE project is embedded in the modular numerical tool Eco3M (Baklouti et al., 2006), which uses mechanistic formulations to describe the biogeochemical processes engaged in the dynamics of marine pelagic ecosystems. Eco3M provides high flexibility by allowing its users to remove or add variables or processes to better adapt the model to a specific study. The VAHINE experiment consisted in the deployment of three replicate mesocosms in New Caledonia. Each mesocosm was modelled through a 1D box model with 14 boxes of 1m height each. Mass transfer between boxes is only allowed through sinking of particulate matter. Until day 10, only the detrital particles are allowed to sink but after this date, 10 % of all the living and non-living dissolved and particulate compartments are allowed to sink. This aims at representing the setting of the aggregation process and the subsequent intensification of the sinking process. The aggregation process was indeed supposed to be favored, not only by the reduced eddy fluxes due to the containment of water, but also by the release of TEP (Berman-Frank et al., subm., this issue). At the bottom of the modelled mesocosms, the sinking material is cumulated to be compared with the particulate matter collected daily in the traps. Sinking velocities were not measured during the experiment, and the matter daily collected in traps was used to parameterize the sinking velocity. The latter is therefore set constant until day 10 at 0.7 m.day^{-1} and increases through the polynomial function given by equation (1) to reach 10 m.day^{-1} at the end of the simulation :

$$V = \alpha * t^{10} + \beta \quad (1)$$

$$\alpha = \frac{(V_{max} - V_{min})}{t_{end}^{10} - t_{ini}^{10}} \quad (2)$$

$$\beta = V_{min} - \alpha * t_{ini}^{10} \quad (3)$$

where V is the sinking velocity, V_{min} and V_{max} are respectively the minimum and maximum sinking velocities (0.7 and 10 m.d^{-1}), t is time, t_{ini} is the moment at which sinking rate starts to increase (i.e. day 10) and t_{end} is the final day of the run (i.e. day 25). The VAHINE data also revealed that the water column inside the mesocosms was well mixed (Bonnet et al. (b), subm., this issue), probably through natural convection at night. This feature is simply modeled through a vertical homogenization of every concentration once a day (at midnight), by imposing the vertically-averaged concentrations in each box. Light irradiance data from the nearest meteorological station (Noumea airport)



were used for the surface irradiance in the model, and a vertical gradient was simulated thanks to a classical Beer-Lambert law using the attenuation coefficient found in Morel (1988). When the total N and P pools (N_{total} and P_{total}) were calculated with the model outputs and compared to those obtained *in situ*, a significant difference appeared regarding P_{total} , while the N_{total} fitted well (data not shown). This gap was mainly due to a DIP concentration that was too high compared to data, indicating a non-total consumption by organisms (not shown). To deal with this DIP excess in the system, a loss of DIP was added to the model. The main hypothesis to explain this DIP loss without a similar loss in DIN is the formation of a biofilm of N_2 -fixing organisms on the walls of the mesocosms (see Knapp et al. (subm., this issue) for details and DIP consumption calculations by the biofilm). Based on Knapp et al. (subm., this issue) calculations, this loss was estimated to $10 \text{ \%} \cdot \text{d}^{-1}$ and was assumed to have no influence on primary, bacterial or export production.

2.3 The biogeochemical model

The biogeochemical model used in this study is based on the Eco3M-MED model used for the Mediterranean Sea (Alekseenko et al., 2014). The only modification made on this previous version lies in the addition of diazotrophs and N_2 fixation process to adapt the model to the VAHINE experiment. The model includes 8 Planktonic Functional Types (PFT): four primary producers (autotroph phytoplankton), three consumers (zooplankton) and one decomposer (heterotrophic bacteria). All of them are represented in terms of several concentrations (C, N, P and chlorophyll concentrations for phytoplankton) and abundances (cells or individual per liter) (Mauriac et al., 2011). Phytoplankton is originally divided into two size-classes, namely the large phytoplankton ($\geq 10 \mu\text{m}$) (PHYL) and the small phytoplankton ($\leq 10 \mu\text{m}$) (PHYS). The two N_2 -fixing organisms are also distinguished by their size, the large one representing *Trichodesmium* sp. (TRI) and the small one *Cyanothece* sp. (UCYN-C), which highly developed in the mesocosms during the experiment (Turk-Kubo et al., 2015). The zooplankton compartment is also divided in the three size classes, nano-, micro- and mezo-zooplankton, which respectively represent heterotrophic nanoflagellates (HNF), ciliates (CIL) and copepods (COP). The latter is represented in terms of abundance and C, N, P concentration. This differs from the model described in Alekseenko et al. (2014), in which meso-zooplankton is only represented through an abundance and a C concentration. Three nutrients are considered, namely nitrate (NO_3^-), ammonium (NH_4^+) and phosphate (DIP). The dissolved organic pool (DOM) is composed of labile and semi-labile fractions of DOC (LDOC and SLDOC), and labile fractions of DON and DOP (LDON and LDOP). The refractory organic pools are not represented. Finally, the detrital particulate matter is represented in terms of C, N and P (Det_C , Det_N and Det_P). All the biogeochemical processes and interactions between the state variables are described in Fig. 1. Except for the new parameters associated with the new features of the model as compared to the original one (Alekseenko et al., 2014), the common parameters between the two model versions are identical.



2.3.1 Initial conditions

Initial values for the model state variables were derived from the *in situ* measurements averaged
 165 over the three mesocosms and the three sampling depths (1m, 6m, 12m). Measured DOM values
 included the refractory organic matter while the model only represents the labile (and semi-labile for
 C) fraction. To extract the labile fraction from DON data, we considered that the labile DON cor-
 responded to the quantity consumed during the experiment in the mesocosms which was estimated
 at $1 \mu\text{mol.L}^{-1}$. The percentage of the labile portion over the total DON was calculated and then ap-
 170 plied to DOP to estimate the initial concentration of labile DOP. The available DOC fraction (LDOC
 + SLDOC) was evaluated at $5 \mu\text{mol.L}^{-1}$ in the Equatorial Pacific (Pakulski and Benner, 1994).
 PHYL was initialized with diatoms data, and PHYS with the sum of nanoEukaryotes, picoEukary-
 otes, *Synechococcus* sp. and *Prochlorococcus* sp.. The initial detrital particulate matter was derived
 by subtracting the total living particulate matter considered in the model to the total particulate mat-
 175 ter measured *in situ*. Accounting for the lack of data of zooplankton, we initiated the variables using
 different ratios between BAC, HNF and CIL abundances. HNF_{cell} was 50 times less than BAC_{cell}
 and CIL_{cell} was 2500 times less than HNF_{cell} . The standard value of 0.5 ind.L^{-1} was used for adult
 COP_{ind} which is consistent with the recent results of Hunt et al. (subm., this issue). The initial values
 of C, N, P and chlorophyll concentrations for the planktonic compartments were derived from the
 180 initial cellular abundance data and from arbitrarily fixed intracellular contents (table 1).

2.3.2 Modeling N_2 fixation

The mathematical formulation (see Eq. (4)) used to represent N_2 fixation was adapted from Rabouille
 et al. (2006) in order to be compatible with the formalism of the present model. It describes the N_2
 fixation flux as a function of the nitrogenase (i.e. the enzyme catalyzing N_2 fixation) activity (Nase)
 185 and the diazotroph abundance ($\text{DIAZO}_{\text{cell}}$, where DIAZO either refers to TRI or UCYN-C). The
 N_2 fixation flux is regulated by the intracellular C quota and the N:C and P:C ratios (equation (8))
 and by the intracellular N quota and N:C ratio (equation (9)). Intracellular N quota controls the net
 N_2 fixation rate through a quota function ($1-f_{Q_N}$, equation (9)), the N excess exuded being equally
 distributed into the DON and NH_4^+ pools. As in Rabouille et al. (2006), the nitrogenase activity
 190 (Nase, in $\text{molN.cell}^{-1}.\text{s}^{-2}$) is a state variable, which dynamics is described in equation (5). The
 nitrogenase activity results from the balance between the increase and the decrease in its activity.
 The increase in the potential nitrogenase activity is assumed to be controlled by the N intracellu-
 lar quota (equation (6)) and by the NO_3^- concentration in field (equation (7)). *Trichodesmium* are
 non-heterocystous filamentous cyanobacteria with differentiated cells located in the center part of
 195 the colony called diazocysts (Bergman and Carpenter, 1991), where N_2 fixation occurs. This spatial
 segregation mechanism is used by the organism to protect the nitrogenase enzyme from oxygen inac-
 tivation produced by photosynthesis (Carpenter and Price, 1976; Bryceson and Fay, 1981). Besides,



Trichodesmium combines a spatial and temporal segregation to maximize the protection of the nitrogenase. This therefore allows the cells to fix only a few hours in daytime around noon (Roenneberg and Carpenter, 1993; El-Shehawey, 2003; Berman-Frank et al., 2001)). On the contrary, UCYN-C can only use a temporal strategy to separate N_2 fixation and photosynthesis processes and thus need to fix N_2 to protect the nitrogenase from O_2 , released by photosynthesis during the day (Reddy et al., 1993). The inhibition of N_2 fixation during the day for UCYN-C and during the night for TRI is simulated by the f_{inhib} function (equation (10), 12 h lagged between TRI and UCYN-C) which controls the nitrogenase activity. The decrease in nitrogenase activity is regulated by a saturation function involving $Nase_{dec}^{max}$, a coefficient of nitrogenase degradation (see equation (5) and table 2). Both the increase and decrease in nitrogenase are energy dependent and controlled by the intracellular C quota (equation (8)).

$$\underbrace{Flux_{N_2 fix}}_{molN.l^{-1}.s^{-1}} = \underbrace{Nase}_{molN.cell^{-1}.s^{-1}} \times \underbrace{DIAZO_{CELL}}_{cell.l^{-1}} \times f_{Q_C} \times (1 - f_{Q_N}) \quad (4)$$

$$\frac{dNase}{dt} = \underbrace{\overbrace{Nase_{prod}^{max}}^{\text{Maximum rate of increase}} \times \min(f^{Nase}, f^{NO_3^-}) \times f_{Q_C} \times f_{inhib}}_{\text{Increase in Nitrogenase activity}} - \underbrace{\overbrace{Nase_{dec}^{max}}^{\text{Maximum rate of decrease}} \times \frac{Nase}{Nase + K_{Nase}} \times f_{Q_C}}_{\text{Decrease in Nitrogenase activity}} \quad (5)$$

$$f^{Nase} = \min \left(\max \left[\left(\frac{Q_{NC}^{max} - Q_{NC}}{Q_{NC}^{max} - Q_{NC}^{min}} \right)^{0.06}, 0 \right], \left(\frac{Q_N^{max} - Q_N}{Q_N^{max} - Q_N^{min}} \right)^{0.06}, 1 \right] \quad (6)$$

$$f^{NO_3^-} = \frac{1}{1 + \frac{NIT}{K_{NO_3^-}}} \quad (7)$$

$$f_{Q_C} = \max \left(\left[\left(\frac{Q_{NC}^{max} - Q_{NC}}{Q_{NC}^{max} - Q_{NC}^{min}} \right)^{0.06}, 0 \right], \max \left[\left(\frac{Q_{PC}^{max} - Q_{PC}}{Q_{PC}^{max} - Q_{PC}^{min}} \right)^{0.06}, 0 \right], \left(\frac{Q_C - Q_C^{min}}{Q_C^{max} - Q_C^{min}} \right)^{0.06}, 1 \right] \quad (8)$$



$$f_{Q_N} = \begin{cases} 0 & \text{si } Q_N \leq Q_N^{\min} \\ \min \left\{ 1 + \left| \frac{Q_N^{\max} - Q_N}{Q_N^{\max} - Q_N^{\min}} \right|^{0.06}, 2 \right\} & \text{if } Q_N \geq Q_N^{\max} \\ 1 - \left(\frac{Q_{NC}^{\max} - Q_{NC}}{Q_{NC}^{\max} - Q_{NC}^{\min}} \right)^{0.06} & \text{if } Q_N \in [Q_N^{\min}, Q_N^{\max}] \text{ and } Q_{NC} \leq Q_{NC}^{\max} \\ \min \left\{ 1 + \left| \frac{Q_{NC}^{\max} - Q_{NC}}{Q_{NC}^{\max} - Q_{NC}^{\min}} \right|^{0.06}, 2 \right\} & \text{else} \end{cases} \quad (9)$$

$$f_{inhib} = \exp(3.7(\cos(2\pi t - \pi) - 1)) \quad (10)$$

2.3.3 Parametrization of diazotrophs and diazotrophs activity

Trichodesmium sp. and unicellular cyanobacteria (Group C and specially *Cyanothece* sp.) exhibit distinct physiologies, sizes and morphologies. Regarding the parametrization of diazotrophs and the processes they undertake that are common with non-diazotrophs, it has arbitrarily been considered that *Trichodesmium* cells are equivalent to PHYL cells and the TRI state variable was therefore parameterized like 100 PHYL cells (considering that a trichome includes 100 cells, Luo et al. (2012)), and UCYN-C were parameterized like PHYS. For the diazotrophy process, parameters for TRI were configured using the Rabouille et al. (2006) work. TRI was also hypothesized to be not grazed in the field. Its main predator is the copepods from the Harpacticoida order (mostly Macrosetella and Miracia) (O'Neil and Roman, 1992), which are not significantly found in the study area (Hunt et al., subm., this issue). To our knowledge, Grimaud et al. (2013) was the first to propose a dynamical model to depict the N_2 fixation by a unicellular cyanobacteria (UCYN-C, *Crocospaera watsonii*). Nevertheless, since this formulation of N_2 fixation was different from that of Rabouille et al. (2006), we couldn't use the parameters provided in Grimaud et al. (2013). The latter were therefore derived from that of TRI not only on the basis of cell size considerations, but to obtain a global agreement with N_2 fixation fluxes measured during the experiment. All the parameters added for both TRI and UCYN-C new compartments are detailed in table 2.

2.4 The fate of N_2 fixed

The main purpose of the DIP enrichment was to enhance diazotrophy in the mesocosms and facilitate the measurement of the DDN transfer. To follow the pathways of DDN throughout the food web, a post treatment was realized since the model itself does not allow to distinguish between the DDN and other N sources. The post-processing treatment aimed at dynamically calculating the DDN proportion in each compartment of the biogeochemical model. At the beginning of the simulation, we assumed that DDN was equal to zero in each compartment. We further assumed that the ratio DDN/N in each N flux leaving a given compartment was the same as the one within this compartment. DDN transfer starts with N exudation by diazotrophs. This DDN release fueled the DON and



NH_4^+ compartments, which are then taken up by autotrophs and heterotrophs. Grazing by zooplankton on the lower trophic levels will then transfer part of the DDN by excretion, sloppy feeding, and egestion of fecal pellets. Finally, remineralization and natural mortality will also contribute to the transfer of DDN among the planktonic food web. Fig. 2 illustrates the different processes involved in the DDN transfer within the ecosystem.

3 Results

Two simulations of the mesocosm experiment were run: the first one includes the representation of the DIP enrichment (SIM^E), while the second one does not consider this enrichment (SIM^C). The latter simulation can be considered as a proxy of the planktonic dynamics outside the mesocosms in lagoon waters. For the sake of clarity and better readability, prefixes "m" and "o" will be used to refer to model and observations respectively, and a * will be used to notify data measured outside the mesocosms. A vertical homogeneity was observed in the mesocosms during the experiment for most of the biogeochemical and diversity parameters (Berthelot et al. (2015b), Turk-Kubo et al., subm., Leblanc et al., subm., this issue). We thus used the average of the three sampling depths to plot both model results and observations. Three periods (namely P0, P1 and P2) were distinguished during the experiment based on biogeochemical characteristics (Berthelot et al. (2015b), this issue) and on changes in the diazotroph community composition (Turk-Kubo et al., subm., this issue). P0 stands for the few days before the DIP enrichment, P1 for the period just after the enrichment (i.e. from day 5 to day 14), and P2 for the period from day 15 to day 23.

3.1 Dynamics of the different N and P pools

During P0, mDIP in SIM^E decreases slowly from 47 to 24 nmol.L^{-1} (Fig. 3, (a)). In response to the DIP enrichment at the end of day 4, mDIP reaches 830 nmol.L^{-1} , before gradually decreasing to the low concentrations observed before the enrichment (Fig. 3, (a)). During the experiment, the DIP enrichment led to three different oDIP in the 3 mesocosms with 740, 780 and 990 nmol.L^{-1} in M1, M2 and M3, respectively, reflecting the slightly different volumes of the mesocosms (Bonnet et al. (b), subm., this issue). oDIP then decreased below the quantification limit of 50 nmol.L^{-1} in the three mesocosms but the consumption of oDIP in M1 was the fastest and those in M2 the slowest. Without the DIP enrichment (SIM^C), mDIP is quickly consumed and the concentrations remain close to zero until the end of the simulation, consistent with oDIP* which was < 50 nmol.L^{-1} all along the experiment.

As for oNH_4^+ , nmNH_4^+ remains low and stable around 15 nmol.L^{-1} over the experiment (not shown here). mNO_3^- also fits well with oNO_3^- , with nearly constant concentrations close to the quantification limit of 50 nmol.L^{-1} (Fig. 3, (b)) over the whole experiment.

oDOP and oDON remained relatively stable throughout the experiment with values around 5 $\mu\text{mol.L}^{-1}$



and $0.14 \mu\text{mol.L}^{-1}$, respectively, with a slight decrease in P2 at the end (Fig. 3, (c) and (d)). A slight increase in mDOP in SIM^E and a slight decrease in both mDOP and mDON are observed during P2. For SIM^C , mDOP and mDON remain stable throughout the simulated period (Fig. 3, (c) and (d)).

280 The trend was similar for oPOP and oPON with constant concentrations or a slight decrease during P1, followed by a large increase (by a factor of 1.5, 1.5 and 2 in M1, M2 and M3, respectively, in oPON, and by a factor of 1.4, 1.4 and 2.4 in M1, M2 and M3, respectively, in oPOP) during P2 (Fig. 3, (e) and (f)). SIM^E results are in good agreement with data for mPON which starts at $1 \mu\text{mol.L}^{-1}$ and then increases to a maximum of $1.5 \mu\text{mol.L}^{-1}$ during P2. While oPOP decreased

285 slightly at the beginning of P1 and increased during P2, mPOP in SIM^E remains constant ($0.08 \mu\text{mol.L}^{-1}$) from day 5 to 10 and increases after day 10. The increase in mPOP up to the $0.14 \mu\text{mol.L}^{-1}$ peak is higher and occurs earlier than oPOP, before to decrease as in the observed data at the end of P2. In SIM^C , the total particulate organic matter falls down throughout the entire simulation, from 0.06 to $0.02 \mu\text{mol.L}^{-1}$ for mPOP, and from 1 to $0.4 \mu\text{mol.L}^{-1}$ for mPON.

290 oN_{total} averaged $6.2 \mu\text{mol.L}^{-1}$ during P1 and started to decrease at the end of P2 in the mesocosms (Fig. 3, (h)). mN_{total} in both SIM^E and SIM^C are quite similar and in the same range as the one observed in data, with a decrease a bit stronger for SIM^C at the end of P2. SIM^E shows an immediate and high increase in mP_{total} ($1\text{--}1.2 \mu\text{mol.L}^{-1}$) on day 5, corresponding to the DIP enrichment, while mP_{total} in SIM^C is constant (250 nmol.L^{-1}) throughout the simulation (Fig. 3, (g)). After the

295 enrichment, mP_{total} starts to decrease down to $0.2\text{--}0.25 \mu\text{mol.L}^{-1}$ on day 22. oChl remained stable during P1 and increased during P2 by a factor of 5 up to a maximum of $1 \mu\text{g.L}^{-1}$ in M3 (Fig. 4 (a)). oChl a was lower ($0.6 \mu\text{g.L}^{-1}$) in M1 and M2 at the end of P2. mChl a calculated by SIM^E is similar to oChl a in M1 and M2, with a decrease a little more marked during P1 and a maximum of $0.5 \mu\text{g.L}^{-1}$ in P2. When mChl a increases during P2 in SIM^E , mChl a in SIM^C remains stable

300 ($\sim 0.1 \mu\text{g.L}^{-1}$) until the end of the simulation.

3.2 Dynamics of the different fluxes

The biogeochemical fluxes relative to the main processes like primary and bacterial productions (PP and BP), N_2 fixation (N_2^{fix}), turnover time of DIP (T_{DIP}) and particulate matter export fluxes (POC_{exp} , PON_{exp} and POP_{exp}) have been calculated by the model and compared to the measured

305 ones (Fig. 4 (b) to (h)).

At the beginning of P0, oN_2^{fix} as well as mN_2^{fix} (both in SIM^E and SIM^C) were about $17 \text{ nmolN.L}^{-1}.\text{d}^{-1}$ and declined gradually during P1 down to $10 \text{ nmolN.L}^{-1}.\text{d}^{-1}$. While mN_2^{fix} in SIM^C continues to decrease during P2, mN_2^{fix} in SIM^E increases during P2 by a factor of 4, consistent with oN_2^{fix} , and reaching a maximum of $42 \text{ nmolN.L}^{-1}.\text{d}^{-1}$ on day 23. PP and BP exhibited the same temporal

310 dynamics in both data and SIM^E results. They first slightly decrease before the DIP enrichment, remain stable during P1 and increase during P2 by a factor of 4.4 and 2.7, for PP and BP, respectively (Fig. 4, (c) and (e)). During P2, mPP (SIM^E) rises until $2 \mu\text{molC.L}^{-1}.\text{d}^{-1}$, which is in the



range of the oPP measured in the three mesocosms. M3 exhibited higher values of oPP than those in M1 and M2 during P2 (around $4 \mu\text{molC.L}^{-1}.\text{d}^{-1}$ on day 22). Even if mBP (in SIM^E and SIM^C) starts at a higher rate than oBP measured in the 3 mesocosms, it decreases rapidly from day 2 to 4 to reach the *in situ* value before the enrichment. The increase in mBP from day 11 to day 17 in SIM^E is a bit overestimated compared to data. BP then better fits the data measured at the end of P2, and especially in M3 ($500 \text{ ngC.L}^{-1}.\text{h}^{-1}$). In SIM^C , the increase in mBP and mPP during P2 does not occur and these rates remain constant around $0.5 \mu\text{molC.L}^{-1}.\text{d}^{-1}$ for mPP and $200 \text{ ngC.L}^{-1}.\text{h}^{-1}$ for mBP throughout the 25 days of the simulation. mBP values in SIM^C are lower than the ones measured in the three mesocosms and consistent with the oBP values measured in lagoon waters (Fig. 4, (e)). T_{DIP} is a relevant indication of DIP availability in the water column. After a slight decline of oT_{DIP} during P0 to values lower than 1 day, T_{DIP} increased dramatically up to 30 days (oT_{DIP}) and 21 days (mT_{DIP}) after the DIP enrichment. mT_{DIP} then decreases linearly in SIM^E as well as oT_{DIP} , in the 3 mesocosms. mT_{DIP} in SIM^C has the same trend as the oT_{DIP} measured in the lagoon waters (Fig. 4, (g)).

The fluxes of exported matter POC_{exp} , PON_{exp} and POP_{exp} for C, N and P respectively are represented in Fig. 4, (d), (f) and (h) in terms of dry matter measured in the sediment traps (Berthelot et al., 2015b). During P1, the daily export remains relatively stable and averaged 18, 1.13 and 0.09 mmol for $m\text{POC}_{exp}$, $m\text{PON}_{exp}$ and $m\text{POP}_{exp}$, respectively. $o\text{POC}_{exp}$, $o\text{PON}_{exp}$ and $o\text{POP}_{exp}$ gradually increased during P2 (from day 15 to 25) to reach a maximum of 57 mmolC.d^{-1} , 5 mmolN.d^{-1} and 0.5 mmolP.d^{-1} respectively. In SIM^E , $m\text{POC}_{exp}$, $m\text{PON}_{exp}$ and POP_{exp} fit well data with a slight overestimation of $m\text{POP}_{exp}$ at the end of P2 which reaches a maximum of $0.75 \text{ mmolP.d}^{-1}$. There is no significant difference between SIM^E and SIM^C for mC_{exp} and $m\text{PON}_{exp}$, from the beginning of the experiment to the middle of P2 (day 18). From day 19, the increase in $m\text{POC}_{exp}$ and $m\text{PON}_{exp}$ is less important in SIM^C than in SIM^E . For $m\text{POP}_{exp}$, the increase in SIM^E occurs earlier (day 15) and the discrepancy between SIM^E and SIM^C is larger at the end of the simulation.

3.3 Evolution of planktonic abundances

The model also simulates the abundances of organisms in cell.L^{-1} for single-cells, in trichome.L^{-1} for TRI and in ind.L^{-1} for zooplankton, besides being represented in term of biomass (C,N,P and Chl for phytoplankton).

mTRI remains constant in SIM^E around $250 \text{ trichomes.L}^{-1}$. By contrast, a large development of UCYN-C occurs during P2 with $m\text{UCYN-C}$ reaching $5.10^7 \text{ cell.L}^{-1}$ (Fig. 5, (a) and (b)). This increase in $m\text{UCYN-C}$ is consistent with the observed dynamics, though the $m\text{UCYN-C}$ increase is overestimated in SIM^E compared to $o\text{UCYN-C}$. mPHYL decreases over time in both SIM^E and SIM^C (Fig. 5, (c)). In the three mesocosms, oPHYL increased from day 10 to 15 reaching 10^5 cell.L^{-1} before decreasing back to values close to that of mPHYL. During P0, mPHYS decreases slightly like oPHYS. During P1, the decrease in mPHYS (down to $0.1 \cdot 10^8 \text{ cell.L}^{-1}$) is stronger than



that of oPHYS, which increases since day 10 and reaches the same range of values as oPHYS at
 350 the beginning of P2. During P2, mPHYS and oPHYS increase up to $1.5 \cdot 10^8 \text{ cell.L}^{-1}$ for mPHYS
 in SIM^E and $1.3\text{--}2.9 \cdot 10^8 \text{ cell.L}^{-1}$ for oPHYS. While mPHYS are similar in SIM^E and SIM^C from
 day 2 to day 8, the increase in mPHYS after day 8 and until the end of P2 is lower in SIM^C than
 in SIM^E (Fig. 5, (d)). As for PHYS, there is a slight decrease in mBAC and oBAC during P0. The
 DIP enrichment on day 4 leads to a strong decline from day 5 to day 8, which is more marked in
 355 mBAC ($9.5 \cdot 10^7 \text{ cell.L}^{-1}$ in SIM^E) than in oBAC ($2.3\text{--}3.1 \cdot 10^8 \text{ cell.L}^{-1}$). From day 8 to the end
 of the simulation, mBAC increases up to a maximum of $1.1 \cdot 10^9 \text{ cell.L}^{-1}$, while oBAC reached a
 maximum of $6.8\text{--}8.5 \cdot 10^8 \text{ cell.L}^{-1}$ at the end of the experiment. In the same way, mBAC are similar
 in SIM^E and SIM^C from day 2 to day 8, and then increase until the end of the simulation but to a
 lower extent in SIM^C than in SIM^E . Since no zooplankton data that could be used for comparison
 360 with the model results were available, only the dynamics of SIM^E and SIM^C are presented (Fig. 5,
 (g) to (f)). mHNF and mCIL have the same trends though they are time-shifted. mCOP is similar in
 SIM^E and SIM^C , with a decline from 0.5 ind.L^{-1} at the beginning to less than 0.1 ind.L^{-1} at the end
 of the simulation. Except for mCOP and mPHYL, the DIP enrichment has an important impact on
 the plankton dynamics as significant differences between the results of SIM^E and SIM^C in mTRI,
 365 mUCYN-C, mPHYS, mBAC, mHNF and mCIL are observed. Overall, SIM^C presents abundances 3
 to 680 times lower than those simulated by SIM^E , though the temporal trends were similar between
 the two simulations

3.4 DIP enrichment and diazotrophs growth

The model also gives additional information not provided by the data regarding the growth of the
 370 organisms or about their intracellular contents. The population growth rate (in $\text{cell.L}^{-1}.\text{s}^{-1}$) as well
 as the specific growth rate (in s^{-1}) are plotted in Fig. 6 (a) and (b) while the relative intracellular
 C, N and P quotas (i.e. Q_C , Q_N and Q_P) are plotted in Fig. 6 (c) and (d). The DIP enrichment
 at the end of day 4 has a direct impact on Q_P for both TRI and UCYN-C, with an instantaneous
 increase in Q_P up to 100 % on day 5. While Q_C , Q_N and Q_P for TRI remain at their maximum
 375 value until the end, Q_N and Q_C of UCYN-C decrease as soon as Q_P increases on day 5. During
 P2, Q_P gradually declines for TRI and faster for UCYN-C. The reverse process then takes place
 with an increase in Q_N and Q_C for UCYN-C when Q_P decreases since day 15, whereas this is not
 observed for TRI. All along the simulation, the trends of $f_{\text{TRI}^{\text{trich}}}^{\text{growth}}$ and $f_{\text{TRI}}^{\text{growth}}$ are similar, with a
 sudden increase on day 5 followed by rather constant and then decreasing values (Fig. 6 (b)). By
 380 contrast, the increase in $f_{\text{UCYN-C}^{\text{cell}}}^{\text{growth}}$ after the DIP enrichment (day 5) is not observed in $f_{\text{UCYN-C}}^{\text{growth}}$,
 namely at the population scale (Fig. 6 (a)). $f_{\text{UCYN-C}}^{\text{growth}}$ increases 10 days later, i.e. during P2, up to a
 maximum of $200 \text{ cell.L}^{-1}.\text{s}^{-1}$ on day 22.



3.5 Fate of DDN in the ecosystem

The fate of the N that has been fixed since the beginning of the simulation (DDN) has been examined using the post-processing treatment described in the Methods section. In short, the proportion of the total DDN present in each living and non-living compartment of the water column and in the traps was calculated throughout the simulation period (Fig. 7). At the start of the experiment, DDN is nearly exclusively in TRI (the proportion of DDN in UCYN-C is negligible) but this proportion decreases all along the simulation. Until day 10, most of the DDN is transferred to the DON pool (which contains about 35 % of the total DDN on day 10), followed by (in their order of importance) NH_4^+ (up to 10 % on day 5), DET (12 % on day 10), and the components of the microbial loop. Until day 10, the proportion of DDN in each compartment except TRI, either increases with time, or reaches a maximum around day 5, consistent with the decrease in N_2 fixation rates during that period. After day 10, the proportion of DDN increases in all living organisms, thereby indicating the transfer of DDN to non-diazotrophic organisms. DDN proportion increases almost until the end of the simulation in CIL and HNF, but only until day 18 in BAC, PHYS and MZOO before decreasing again. In the non-living compartments, the proportion of DDN decreases after day 10 (day 12 for DON) until the end of the simulation. Finally, the proportion of DDN in traps is almost null during the ten first days of the experiment, before increasing and then stabilizing around 4%. The percentage of DDN with respect to total particulate N contained in the traps has also been plotted (Fig. 8). This percentage increases quite linearly with time from 0 to nearly 0.4 % between day 2 and day 10. On day 10, the percentage increases much more rapidly until day 12 and then rises gradually to a plateau around 1.2 % before increasing again at the very end of the experiment.

4 Discussion

N input by N_2 fixation in the upper SW Pacific Ocean is thought to be controlled by DIP availability because of the presence of depleted trace metals concentrations compared to the adjacent South Pacific central gyre Moutin et al. (2005, 2008)). The aim of the VAHINE experiment (Bonnet et al., b) (this issue) was to (i) investigate the fate of the DDN in oligotrophic ecosystems by removing any potential DIP limitation for diazotrophs and thereby potentially stimulate the growth of organisms (in particular diazotrophs), (ii) enhance N_2 fixation and DDN fluxes through the entire ecosystem, and (iii) study the dynamics of biogeochemical C, N, P fluxes. N_2 fixation is expected to rapidly deliver new N to other organisms than diazotrophs, thus reducing possible N growth limitation or co-limitation in the ecosystem. Our goal was to follow the dynamics of this new N toward the food chain, the inorganic and organic N pools, as well as in the exported particulate matter. The discussion will concern expected and unexpected results obtained in this study after the DIP enrichment, as well as the fate of DDN in the ecosystem.



4.1 An expected enhancement of biogeochemical fluxes after the DIP enrichment

The mesocosms DIP enrichment performed at the end of day 4 associated with the provision of new N by diazotrophy led to a large increase in diazotrophs (especially UCYN-C) abundances (Fig. 5, (a) and (b))), biomass (data not shown) and N_2 fixation fluxes during P2, and a significant development of UCYN-C occurred during that period. Whereas a large increase in N_2 fixation is observed in SIM^E during P2 (consistent with the data indicating a near three-fold higher mean N_2 fixation rate in P2 than P1) (Fig. 4, (a)), N_2 fixation rates gradually decreases in SIM^C , indicating strong differences between the mesocosms conditions and those encountered in lagoon waters. Hydrological parameters such as temperature and biogeochemical conditions were all similar inside and outside the mesocosms, except the DIP conditions (Bonnet et al. (b),subm., this issue), confirming that the DIP enrichment stimulated N_2 fixation in this experiment. Nevertheless, a slight increase in N_2 fixation rates was observed outside the mesocosms during P2 (+35 %), which could be explained by a provision of external DIP sources to the lagoon, by growth on DOP sources (Dyhrman et al., 2006) and/or by the increasing seawater temperature along the 25-days experiment (Bonnet et al. (b),subm., this issue), which provides favorable conditions for diazotroph growth (Carpenter et al., 2004). A rapid decrease in T_{DIP} was observed on day 5 after the DIP enrichment, suggesting a rapid consumption of the DIP by the planktonic community. Diazotrophs were the first to respond to the DIP enrichment in term of abundance, even if this response did not lead to an immediate increase in the N_2 fixation rate. The latter significantly increased during P2 in relation to the development of UCYN-C (Turk-Kubo et al., subm., this issue). Other autotrophic organisms and heterotrophic bacteria declined until the middle of P1, and started to grow 10 days after the DIP enrichment (except PHYL). Despite this time lag between the DIP enrichment and the planktonic response, the DIP enrichment resulted in an increase in the abundances of all planktonic groups except PHYL and COP (Fig. 5). The DIP limitation at the beginning of the experiment is represented in the model by setting the P cell contents of all organisms at their minimum value, which leads to an immediate uptake of DIP after the enrichment at the end of day 4 (Fig. 7, (c) and (d)). At the cellular scale, this immediate DIP uptake results in a fast increase in intracellular P-contents of autotrophs and heterotrophic bacteria up to their maximum quota (Fig. 7, (c) and (d) for diazotrophs). After benefiting diazotrophs, the DDN inputs benefited to non-diazotrophic organisms. Autotrophic PP and heterotrophic BP increased in the model after the DIP enrichment (+262 % and +181 %, from day 5 to day 23, for PP and BP, respectively). The enhanced PP (Fig. 5, (e)) leads to an increase in total suspended matter (Fig 3, (e) and (f)), and finally in exported particulate material (Fig. 5, (d), (f) and (h)). The contribution of N_2 fixation to PP (up to 10.0 % for SIM^E and 6.0 % for SIM^C) is in good agreement with corresponding measured contributions which were equal to 10.9 ± 5.0 % inside the mesocosms and 5.7 ± 2.0 % in the lagoon waters (Berthelot et al., 2015b). Hence, the DIP enrichment not only stimulates N_2 fixation and PP but also the percentage of PP sustained by N_2 fixation. The newly synthesized biomass has two possible fates, namely remineralization or export.



As the model does not represent the diatom-diazotroph associations (DDAs), which were the most
 455 abundant diazotrophs in the mesocosms during P1 (Turk-Kubo et al., subm., this issue), the modeled
 export is probably underestimated during P1. Berthelot et al. (2015b) (this issue) have shown that
 the growth of DDAs during P1 did not lead to a significant increase in POC because DDAs rapidly
 settled down (Villareal et al., 1996) through the water column and the DDN did not benefit to the
 system. This may explain why the export during P1 was lower than during P2, during which we
 460 observed a higher increase in suspended particulate matter (Fig. 5, (d), (f) and (h)) enhanced by the
 UCYN-C growth. Moreover, the presence of large (100-500 μm) UCYN-C aggregates in the meso-
 cosms facilitated their export into the traps (UCYN-C accounted for up to 22.4 ± 4.0 % of total C
 export at the height of their large development (Bonnet et al. (a), subm., this issue). This indicates
 that UCYN-C can not only contribute to direct export but promote indirect export. The high content
 465 of TEP measured in traps on days 15 and 16 (Berman-Frank et al., subm., this issue) in correlation
 with the increase in UCYN-C abundances (Turk-Kubo et al., subm., this issue) leads to the assump-
 tion that the presence of TEP in the field would facilitate export flux and specially the sinking of
 UCYN-C during P2. This phenomenon was taken into account in the model by allowing, each day
 from day 10, the settling of 10 % of all the model compartments (living and non-living, particulate
 470 and dissolved) in addition to the detrital particulate matter. C, N, P export in SIM^E closely follows
 the mesocosm trap measurements (Fig. 6, (d), (f) and (h)). SIM^E shows higher C, N, P exports (+
 28 %, + 35 % and + 158 %, respectively) compared to SIM^C . Large size N_2 -fixing organisms are
 known to directly contribute to C export in coastal and oceanic environments (Subramaniam et al.,
 2008; Karl and Letelier, 2008) but small-size UCYN-C (despite very few studies have focused on
 475 them) were considered as less efficient at promoting export due to their small size (typically 1-6 μm)
 associated with low individual sinking rates, and the tight grazing control that leads to high recycling
 rates in the euphotic zone. In the present study, both our experimental and model results indicate that
 UCYN-C also significantly contribute to export under DIP repleted conditions, both directly by the
 sinking of UCYN-C cells, and indirectly after the transfer of DDN to non-diazotrophic plankton,
 480 which is subsequently exported.

4.2 An unexpected delay for UCYN-C development and biogeochemical fluxes enhancement

The new N provided by N_2 fixation after the DIP enrichment resulted in high PP and BP rates, as well
 as in an increase in export and planktonic abundances. However, these responses were not observed
 immediately after the DIP enrichment on day 4 but 10 days later (Fig. 3 and Fig. 5). The massive
 485 UCYN-C development indeed occurred during P2, with a maximum population growth on day 21
 in the model, consistent with the observation of the maximum in the UCYN-C abundances on days
 20, 16 and 19 in M1, M2, and M3 respectively (Fig. 5, (b)) (Turk-Kubo et al., subm., this issue).
 Which factor may explain the 10 days delay between the DIP enrichment and the large UCYN-C
 development?



At the cellular scale (Fig. 6, (a)), the DIP enrichment has an immediate influence on cell-specific growth rate of UCYN-C, with a 4-fold increase in few hours. However, this immediate response is not observed at the population scale (Fig. 6, (a)). At the beginning of the simulation, P cell quota of UCYN-C is minimum and their cell specific growth rate is therefore equal to zero. Though DIP and DOP are very low at the beginning of the simulation, UCYN-C can however take up part of this available P, thereby increasing their P quota and their growth rate. UCYN-C reach their maximum cellular P quota the day after the DIP enrichment (Fig. 6, (c)) and DIP will not limit the UCYN-C growth anymore until day 17. The peak in cell-specific growth rate at day 5 (Fig. 6, (c)) corresponds to the temporary absence of significant nutrient limitation, while oscillations during the following days correspond to the day/night rhythm in UCYN-C C quota associated with C starvation during night (the specific growth rate is modulated by the lowest intracellular quota). When C is the most limiting nutrient, the night/day oscillations are passed on growth rate. The high increase in cell-specific growth rate on day 5 leads to an increase in UCYN-C abundances (Fig. 5, (b)). After day 5, photosynthesis and N uptake are then not rapid enough to sustain the increased C and N needs, and N, and mostly C at night, become limiting (Fig. 6, (c)). As a consequence, UCYN-C cell-specific growth rate decreases slightly after day 5, and more rapidly after day 18 when DIP becomes once again limiting (Fig. 6, (a)). Fig. 6 illustrates the time lag between the variations at the cellular level for specific growth rate and growth at the population level. The growth rate of the UCYN-C population also increases from the beginning of the simulation since the specific growth rate and the abundance of UCYN-C increase, but this is almost imperceptible until the exponential increase starting around day 11. From day 18, when the specific growth rate begins to strongly decrease, the population growth rate still increases but more slowly and finally decreases after the maximum of $5 \cdot 10^7 \text{ cell.L}^{-1} \cdot \text{s}^{-1}$ reached on day 22 (Fig. 6, (a)). TRI abundance is less influenced by the DIP enrichment than UCYN-C abundance. However, the DIP enrichment leads to an increase in TRI growth rate on day 5 at both the population and the trichome scale (Fig. 6, (c)). Since a trichome includes 100 cells of *Trichodesmium*, the time lag between the responses at the trichome and population levels is therefore far less than the one evidenced for UCYN-C. Furthermore, despite TRI growth is not nutrient-limited from day 5 to day 15 as the three cellular quotas (C, N and P) are at their maximum value (Fig. 6, (d)), TRI population does not increase significantly because of its low maximum division rate as compared to the time scale of the experiment (3 weeks) (consistently with *in situ* data). The aforementioned time lag between cellular and population responses is also useful for understanding what may be viewed as a contradiction: on one hand, we observed a clear and net increase in PP, BP and export productions after the DIP enrichment, both in the mesocosms and in the SIM^E, but on the other hand, oligotrophic waters are generally known to be more DIN than DIP limited. After reviewing the main studies conducted on nutrients limitation, and especially on N and P limitation in oligotrophic waters, Moore et al. (2013) concluded that N was the first limiting nutrient for phytoplankton in nutrient-depleted areas as nutrient-addition experiments did not lead



to a significant increase in autotrophic activity after P additions, whereas it did after N additions (Thingstad et al., 2005; Moore et al., 2008; Tanaka et al., 2011; Zohary et al., 2005). Similar results were obtained in the South Pacific gyre for autotrophs (Bonnet et al. (2008)) and heterotrophs (Van Wambeke et al., 2008), as well as at the start of the present mesocosm experiment (before the DIP enrichment), confirming previous studies indicating proximal N limitation of BP (Van Wambeke et al., subm., this issue) at short time scales (days). This apparent contradiction on DIP limitation may therefore be explained by the time duration of the aforementioned DIP enrichment experiments that was not long enough to evidence the response of the planktonic ecosystem. The enrichment mesocosm experiment conducted during the VAHINE project has allowed to follow the ecosystem and the associated biogeochemical fluxes over a longer period of time (23 days) compared to the nutrient-addition experiments cited above. Since we observed the increase in PP and BP only after 10 days in both experimental and simulation results, we may conclude that 10 days are necessary for the newly fixed N by diazotrophs to sustain the observed high production rates, and to see an effective change in the planktonic populations (in term of abundances, structure and function). In the light of the foregoing, two conclusions may therefore be drawn. First, 10 days may be a lower time limit to characterize the real nutrient limiting primary, bacterial and export productions, at least in marine areas where N_2 fixation is a significant process. Therefore, short-term (~ 2 days) nutrient-addition experiments may not be relevant to study nutrient limitation in marine ecosystems. Second, the initial DIP limitation considered in the model clearly indicates that DIP limitation observed at the cellular level does not reflect the response at the population scale (in terms of primary, bacterial and export productions) which may be delayed. Therefore, in order to correctly assess the nutrient limitation during short-term nutrient addition experiments, nutrient limitation diagnostics operating at cellular level (such as enzymatic responses) need to be applied rather than classical measurements of PP or BP increase after the enrichment.

4.3 The fate of DDN in the planktonic ecosystem and exported matter

At the start of the simulation, DDN is nearly exclusively into TRI since the flux of N_2 fixation by UCYN-C is negligible as compared to that of TRI, and the situation reverses at the end of the simulation when UCYN-C abundance becomes predominant. Due to DON exudation and NH_4^+ release by TRI, the proportion of DDN first increases in the DON and NH_4^+ pools, and then in the NO_3^- pool due to nitrification. Before day 10, planktonic organisms do not significantly benefit from the DDN, as its proportion decreases in BAC and PHYS between days 4 and 8 and in HNF between days 6 and 10. For BAC and PHYS, this is mainly due to the decrease (which is overestimated by the model) in abundance of these both groups between days 5 and 8 due to grazing by HNF and CIL. After day 10, the DDN proportion increases in all the non-diazotrophic plankton groups, and decreases meanwhile in the non-living pools, though a bit later (i.e. from day 13) in DON. This decrease in DDN proportion in the non-living pools is both due to the assimilation of mineral and organic nu-



trients by phyto and bacterioplankton, and to the sinking of the produced organic matter through aggregation processes. Since mineral N is first taken up, the uptake of DON occurs later, namely during P2 as shown in Berthelot et al. (2015b) (this issue). As a consequence, the decrease in DDN-DON percentage is also delayed as compared to that of NO_3^- and NH_4^+ . DDN-DET increases quite regularly until day 10 as long as the sinking rate is constant, and then decreases with the increase in this sinking rate. As a result, DDN in the particulate matter collected in traps increases since day 10 up to the end, consistent with the $\delta^{15}\text{N}$ -budget performed by Knapp et al. (subm., this issue), thereby indicating a higher contribution of N_2 fixation to export production during P2 ($56 \pm 24\%$ and up to 80% at the end of the experiment) compared to P1 ($47 \pm 6\%$ and up to 60%). mDON appears to be the pool which mainly benefits from the DDN. This is due to the DON release by diazotrophs, especially TRI which is at its maximum N quota throughout the simulation (Fig. 8, (c) and (d)). Since their maximum cell division rate is low, their N_2 fixation rate is indeed high enough to allow *Trichodesmium* to fulfill their N reserves and reach their maximum N quota (Fig. 6, (d)). The same is not true for UCYN-C for which the division rate (boosted by the P-enrichment) is too high, as compared to their N fixation rate, to reach their N maximum quota. However, in the model, DDN exudation by diazotrophs releases equal amounts of NH_4^+ and DON. During P1, DDN accumulates in DON (nearly up to 40% on day 13) (Fig. 7, (c)) whereas DDN in NH_4^+ decreases rapidly since day 5 as it is immediately used by heterotrophic bacteria and phytoplankton (Fig. 7, (d)). DDN in DON decreases later (i.e. during P2, when the DON pool begins to be used) as the inorganic N pool is depleted. To conclude on this point, though DDN transits in the same proportions in NH_4^+ and DON, it mostly accumulates in DON since DDN- NH_4^+ is taken up more rapidly. Among the living compartments, PHYS, BAC, HNF and CIL were the main beneficiaries of DDN. PHYS and BAC are indeed the main consumers of NH_4^+ and labile DON (while PHYC is not allowed by the model to uptake DON), and HNF and CIL respectively feed on BAC and PHYS, and on PHYS and HNF. DDN therefore mainly transits through the actors of the microbial loop, which is consistent with NanoSIMS measurements performed after 24 h of incubation with $^{15}\text{N}_2$ on water sampled on day 17 showing that $18 \pm 4\%$ of the DDN was found in picophytoplankton against $3 \pm 2\%$ in diatoms (Bonnet et al., a). According to the model, only 5% of the total DDN were recovered in the traps at the end of the simulation. This proportion is likely underestimated by the fact that UCYN-C sinking is probably underestimated in the model. The contribution of UCYN-C to POC export on day 17 during P2 was indeed 0.25% in the model simulation, against up to $22.4 \pm 4.0\%$ in the data during the same period (Bonnet et al. (a), subm., this issue). In the same way, the ratio DDN/total N in traps equals 1% at the end of the simulation, which is dramatically lower than the measured one which is equal to 80% (Knapp et al., subm., this issue). This discrepancy is partially due to the different methodologies used to make these estimations. In the post-processing treatment, we indeed considered that the initial DDN was null in every compartment, which is obviously not true, but this hypothesis was constrained by the fact that the initial DDN in all the model compartments was un-



known, and arbitrary allocations of DDN in compartments would have added additional uncertainty on the model results. As a consequence, our results are necessarily underestimated as compared to the measured ones since the latter include the history of previous N_2 fixation in the field (i.e. before the beginning of the mesocosm experiment). If we consider an initial content of DDN in the traps equals 30 % as measured by Knapp et al. (subm., this issue), the final modeled DDN content would be 31 %, which is still underestimated, but more realistic. This approximation on the initial nil DDN content in organisms is therefore not sufficient to explain the huge difference with observations concerning the DDN proportion in traps. Another source of error lies in the implicit representation of the aggregation process made in this study. It has indeed been considered that from day 10, 10 % of all the model variables are allowed to sink in addition to the detrital particulate compartment. However, it seems that this leads to an underestimation of UCYN-C sinking. As already mentioned, Bonnet et al. (a) (subm., this issue) showed that the UCYN-C contribution to the particulate C collected in traps on day 17 was up to 22.4 ± 4.0 % against 0.25 % for the model. The *in situ* value has been estimated using a value of the intracellular C-content per cell of 22 pgC.cell^{-1} determined according to the measured UCYN-C cell size in the mesocosms and the equations of Verity et al. . However, the modelled C intracellular content of UCYN-C at day 17 is about 150 times lower ($0.13 \text{ pgC.cell}^{-1}$). This difference in UCYN-C C-contents is due to the straightforward hypothesis we made in the model which was to consider the UCYN-C diazotrophs as PHYS. Our aim was indeed to use the same model developed for the oligotrophic ocean and particularly the Mediterranean Sea (Eco3M-MED) in every oligotrophic region of the ocean. Moreover, we considered that it was potentially informative to consider that the diazotrophs added in the model were similar in all points to PHYS and PHYI except that there were able to fix N_2 . In the model, PHYS represents picophytoplankton and the small nanophytoplankton, and its C intracellular content ranges between 0.08 and $0.25 \text{ pgC.cell}^{-1}$, which seems to be an underestimated value for UCYN-C. During the VAHINE experiment, large cells of UCYN-C (size about $5.7 \mu\text{m}$ (Bonnet et al. (b), subm., this issue)) were present with a C content estimated at 22 pgC.cell^{-1} (Bonnet et al. (a), subm., this issue). With the latter C content, we established that the mUCYN-C contribution to export would reach 28 %, a result consistent with the 22.4 ± 4.0 % estimated by Bonnet et al. (a) (subm., this issue). Finally, the overestimation of UCYN-C abundance by the model also supports the idea that UCYN-C sinking is underestimated by the model. The aggregation process induced by TEP (Berman-Frank et al., subm., this issue) or by specific molecules such as extracellular polysaccharides (EPS) (Sohm et al., 2011), which is not explicitly represented in the model, might explain the preferential export of UCYN-C in the mesocosms. Hence, though aggregation is probably overestimated in the mesocosms as compared to natural situations, the contribution of this process seems to be significant in C export. Overall, though the clear underestimation by the model of the UCYN-C sinking and DDN export, the main conclusions delivered by the model concerning the fate of DDN through the planktonic food web remain unchanged.



4.4 Conclusion

The DIP enrichment conducted during the VAHINE mesocosms experiment in the oligotrophic water of the New Caledonia lagoon (SW Pacific Ocean) led to a clear increase in primary, bacterial and export productions. Two simulations, with and without considering the DIP enrichment, were run. Their comparison allowed to quantify the increase in the main biogeochemical fluxes due to the DIP enrichment. This modeling work was also intended to investigate the fate of the N provided by N_2 fixation (i.e. DDN) throughout the planktonic food web. The dynamics of the functional groups provided by the simulation with the DIP enrichment is globally consistent with the measured ones, especially the development of UCYN-C 10 days after the DIP enrichment. The lag time of 10 days (concomitant with the increase in primary, bacterial and export productions) raises the question of the relevance of the classical methods used to quantify primary and bacterial nutrient limitation, at least in areas where N_2 fixation may sustains a large proportion of new PP. This modeling study also allowed to follow the fate of the new N input by N_2 fixation (DDN) in the ecosystem. According to the model, DDN is mainly found in the dissolved pool (NH_4^+ and DON) before benefiting the whole planktonic community. At the end of the simulation, 43 %, 33 %, and 15 % are respectively found in non-diazotroph organisms, UCYN-C and DON, respectively. The exported matter collected in the traps at 15 m depth showed that export is essentially due to the sinking of small organisms. Although the measured and simulated C, N, P export are consistent in magnitude, the simulated percentage of DDN in traps is significantly lower than that of experimental measurements. During the experiment, UCYN-C export was high, probably due to their aggregation in larger particles thanks to the secretion of TEP or EPS which increased their own sinking velocity rather than the sinking velocity of the whole suspended matter as considered in the present model. Directly or indirectly, small diazotrophs significantly contribute to the particulate export through the aggregation process which needs to be further investigated in future work.



References

- Alekseenko, E., Raybaud, V., Espinasse, B., Carlotti, F., Queguiner, B., Thouvenin, B., Garreau, P., and Baklouti, M.: Seasonal dynamics and stoichiometry of the planktonic community in the NW Mediterranean Sea; a 3D modeling approach, *Ocean Dynamics*, 64, 179–207, 2014.
- 665 Baklouti, M., Faure, V., Pawlowski, L., and Sciandra, A.: Investigation and sensitivity analysis of a mechanistic phytoplankton model implemented in a new modular numerical tool (Eco3M) dedicated to biogeochemical modelling, *Progress in Oceanography*, 71, 34–58, doi:10.1016/j.pocean.2006.05.003, 2006.
- Benavides, M., Agawin, N., Aristegui, J., Penne, J., and Stal, L.: Dissolved organic nitrogen and carbon release by a marine unicellular diazotrophic cyanobacterium, *Aquat Microb Ecol*, 69, 2013a.
- 670 Benavides, M., Bronk, D. A., Agawin, N. S. R., Pérez-Hernández, M. D., Hernández-Guerra, A., and Aristegui, J.: Longitudinal variability of size-fractionated N_2 fixation and DON release rates along 24.5°N in the subtropical North Atlantic: N_2 Fixation in the North Atlantic, *Journal of Geophysical Research: Oceans*, 118, 3406–3415, doi:10.1002/jgrc.20253, 2013b.
- Bergman, B. and Carpenter, E. J.: Nitrogenase confined to randomly distributed trichomes in the marine cyanobacterium *Trichodesmium thiebautii*, *Journal of Phycology*, 27, 158–165, doi:10.1111/j.0022-3646.1991.00158.x, 1991.
- 675 Berman-Frank, I., Spungin, D., Rahav, E., Van Wambeke, F., Turk-Kubo, K., and Moutin, T.: Dynamics of transparent exopolymer particles (TEP) during the VAHINE mesocosm experiment in the New Caledonia lagoon, *Biogeosciences*, subm.
- 680 Berman-Frank, I., Lundgren, P., Chen, Y.-B., Küpper, H., Kolber, Z., Bergman, B., and Falkowski, P.: Segregation of nitrogen fixation and oxygenic photosynthesis in the marine cyanobacterium *Trichodesmium*, *science*, 294, 1534–1537, 2001.
- Berthelot, H., Bonnet, S., Camps, M., Grosso, O., and Moutin, T.: Assessment of the dinitrogen released as ammonium and dissolved organic nitrogen by unicellular and filamentous marine diazotrophic cyanobacteria grown in culture, *Frontiers in Marine Science*, 2, doi:10.3389/fmars.2015.00080, 2015a.
- 685 Berthelot, H., Moutin, T., L'Helguen, S., Leblanc, K., Hélias, S., Grosso, O., Leblond, N., Charrière, B., and Bonnet, S.: Dinitrogen fixation and dissolved organic nitrogen fueled primary production and particulate export during the VAHINE mesocosms experiment (New Caledonia lagoon), *Biogeosciences Discussions*, 12, 4273–4313, doi:10.5194/bg-12-4273-2015, 2015b.
- 690 Biegala, I. C. and Raimbault, P.: High abundance of diazotrophic picocyanobacteria ($<3 \mu m$) in a South-west Pacific coral lagoon, *Aquatic microbial ecology*, 51, 45–53, 2008.
- Bonnet, S., Berthelot, H., Turk-Kubo, K., Fawcett, S., Rahav, E., and L'Helguen, S.: Dynamics of N_2 fixation and fate of diazotroph-derived nitrogen during the VAHINE mesocosm experiment, *Biogeosciences*, subm., a.
- 695 Bonnet, S., Moutin, T., Rodier, M., Grisoni, J., Louis, F., Folcher, E., Bourgeois, B., Boré, J., and Renaud, A.: Introduction to the project VAHINE : VARIability of vertical and troPHic transfer of diazotroph derived nitrogen in the south wEst Pacific, *Biogeosciences*, subm., b.
- Bonnet, S., Guieu, C., Bruyant, F., Prášil, O., Van Wambeke, F., Raimbault, P., Moutin, T., Grob, C., Gorbunov, M. Y., Zehr, J. P., and others: Nutrient limitation of primary productivity in the Southeast Pacific (BIOSOPE cruise), *Biogeosciences*, 5, 215–225, 2008.
- 700



- Bonnet, S., Rodier, M., Turk-Kubo, K. A., Germineaud, C., Menkes, C., Ganachaud, A., Cravatte, S., Raimbault, P., Campbell, E., Quéroué, F., Sarthou, G., Desnues, A., Maes, C., and Eldin, G.: Contrasted geographical distribution of N₂ fixation rates and nifH phylotypes in the Coral and Solomon Seas (South-Western Pacific) during austral winter conditions, *Biogeochem. Cycles*, 2015.
- 705 Bryceson, I. and Fay, P.: Nitrogen fixation in *Oscillatoria* (*Trichodesmium*) *erythraea* in relation to bundle formation and trichome differentiation, *Marine Biology*, 61, 159–166, doi:10.1007/BF00386655, 1981.
- Carpenter, E. J. and Price, C. C.: Marine oscillatoria (*Trichodesmium*): explanation for aerobic nitrogen fixation without heterocysts, *Science*, 191, 1278–1280, doi:10.1126/science.1257749, 1976.
- Carpenter, E. J., Subramaniam, A., and Capone, D. G.: Biomass and primary productivity of the cyanobacterium *Trichodesmium* spp. in the tropical N Atlantic ocean, *Deep Sea Research Part I: Oceanographic Research Papers*, 51, 173–203, doi:10.1016/j.dsr.2003.10.006, 2004.
- 710 Dupouy, C., Neveux, J., Subramaniam, A., Mulholland, M. R., Montoya, J. P., Campbell, L., Carpenter, E. J., and Capone, D. G.: Satellite captures *Trichodesmium* blooms in the southwestern tropical Pacific, *EOS, Transactions American Geophysical Union*, 81, 13–16, 2000.
- 715 Dutkiewicz, S., Ward, B. A., Monteiro, F., and Follows, M. J.: Interconnection of nitrogen fixers and iron in the Pacific Ocean: Theory and numerical simulations, *Global Biogeochemical Cycles*, 26, doi:10.1029/2011GB004039, 2012.
- Dyhrman, S. T., Chappell, P. D., Haley, S. T., Moffett, J. W., Orchard, E. D., Waterbury, J. B., and Webb, E. A.: Phosphonate utilization by the globally important marine diazotroph *Trichodesmium*, *Nature*, 439, 68–71, 2006.
- 720 El-Shehawey, R.: Diurnal expression of *hetR* and diazocyte development in the filamentous non-heterocystous cyanobacterium *Trichodesmium erythraeum*, *Microbiology*, 149, 1139–1146, doi:10.1099/mic.0.26170-0, 2003.
- Fennel, K., Spitz, Y. H., Letelier, R. M., Abbott, M. R., and Karl, D. M.: A deterministic model for N₂ fixation at stn. ALOHA in the subtropical North Pacific Ocean, *Deep Sea Research Part II: Topical Studies in Oceanography*, 49, 149–174, 2001.
- 725 Garcia, N., Raimbault, P., and Sandroni, V.: Seasonal nitrogen fixation and primary production in the Southwest Pacific: nanoplankton diazotrophy and transfer of nitrogen to picoplankton organisms, *Marine Ecology Progress Series*, 343, 25–33, doi:10.3354/meps06882, 2007.
- 730 Glibert, P. M. and Bronk, D. A.: Release of dissolved organic nitrogen by marine diazotrophic cyanobacteria, *Trichodesmium* spp., *Applied and Environmental microbiology*, 60, 3996–4000, 1994.
- Goebel, N. L., Edwards, C. A., Church, M. J., and Zehr, J. P.: Modeled contributions of three types of diazotrophs to nitrogen fixation at Station ALOHA, *The ISME journal*, 1, 606–619, 2007.
- Graziano, L., Geider, R., Li, W., and Olaizola, M.: Nitrogen limitation of North Atlantic phytoplankton: Analysis of physiological condition in nutrient enrichment experiments, *Aquatic Microbial Ecology*, 11, 53–64, 1996.
- 735 Grimaud, G. M., Dron, A., Rabouille, S., Sciandra, A., Bernard, O., and others: Modelling light-dark regime influence on the carbon-nitrogen metabolism in a unicellular diazotrophic cyanobacterium, in: CAB, 2013.
- Gruber, N. and Galloway, J. N.: An Earth-system perspective of the global nitrogen cycle, *Nature*, 451, 293–296, doi:10.1038/nature06592, 2008.
- 740



- Hewson, I., Govil, S. R., Capone, D. G., Carpenter, E. J., and Fuhrman, J. A.: Evidence of Trichodesmium viral lysis and potential significance for biogeochemical cycling in the oligotrophic ocean, *Aquatic Microbial Ecology*, 36, 1–8, 2004.
- Hunt, B., Bonnet, S., Berthelot, H., Conroy, B., Foster, R. A., and Pagano, M.: Contribution and pathways of
745 diazotroph derived nitrogen to zooplankton during the VAHINE mesocosm experiment in the oligotrophic
New Caledonia lagoon, *Biogeosciences*, subm.
- Karl, D. and Letelier, R.: Nitrogen fixation-enhanced carbon sequestration in low nitrate, low chlorophyll
seascapes, *Marine Ecology Progress Series*, 364, 257–268, doi:10.3354/meps07547, 2008.
- Karl, D. M., Bates, N. R., Emerson, S., Harrison, P. J., Jeandel, C., Llinàs, O., Liu, K.-K., Marty, J.-C., Michaels,
750 A. F., Miquel, J. C., Neuer, S., Nojiri, Y., and Wong, C. S.: Temporal Studies of Biogeochemical Processes
Determined from Ocean Time-Series Observations During the JGOFS Era, in: *Ocean Biogeochemistry*,
edited by Fasham, M. J. R., pp. 239–267, Springer Berlin Heidelberg, Berlin, Heidelberg, 2003.
- Karl, D. M., Church, M. J., Dore, J. E., Letelier, R. M., and Mahaffey, C.: Predictable and efficient carbon se-
questration in the North Pacific Ocean supported by symbiotic nitrogen fixation, *Proceedings of the National*
755 *Academy of Sciences*, 109, 1842–1849, 2012.
- Knapp, A. N., Fawcett, S. E., Martinez-Garcia, A., Leblond, N., Moutin, T., and Bonnet, S.: Nitrogen isotopic
evidence for a shift from nitrate- to diazotroph-fueled export production in VAHINE mesocosm experiments,
Biogeosciences, subm.
- Konno, U., Tsunogai, U., Komatsu, D. D., Daita, S., Nakagawa, F., Tsuda, A., Matsui, T., Eum, Y.-J., and
760 Suzuki, K.: Determination of total N₂ fixation rates in the ocean taking into account both the particulate
and filtrate fractions, *Biogeosciences*, 7, 2369–2377, doi:10.5194/bg-7-2369-2010, 2010.
- Leblanc, K., Cornet, V., Caffin, M., Rodier, M., Desnues, M., Berthelot, H., Turk-Kubo, K. A., and Heliou, J.:
Phytoplankton community structure in the VAHINE MESOCOSM experiment, *Biogeosciences*, subm.
- Luo, Y.-W., Doney, S. C., Anderson, L. A., Benavides, M., Berman-Frank, I., Bode, A., Bonnet, S., Boström,
765 K. H., Böttjer, D., Capone, D. G., Carpenter, E. J., Chen, Y. L., Church, M. J., Dore, J. E., Falcón, L. I.,
Fernández, A., Foster, R. A., Furuya, K., Gómez, F., Gundersen, K., Hynes, A. M., Karl, D. M., Kitajima,
S., Langlois, R. J., LaRoche, J., Letelier, R. M., Marañón, E., McGillicuddy, D. J., Moisander, P. H., Moore,
C. M., Mourinho-Carballido, B., Mulholland, M. R., Needoba, J. A., Orcutt, K. M., Poulton, A. J., Rahav,
E., Raimbault, P., Rees, A. P., Riemann, L., Shiozaki, T., Subramaniam, A., Tyrrell, T., Turk-Kubo, K. A.,
770 Varela, M., Villareal, T. A., Webb, E. A., White, A. E., Wu, J., and Zehr, J. P.: Database of diazotrophs
in global ocean: abundance, biomass and nitrogen fixation rates, *Earth System Science Data*, 4, 47–73,
doi:10.5194/essd-4-47-2012, 2012.
- Mahaffey, C., Michaels, A. F., and Capone, D. G.: The conundrum of marine N₂ fixation, *American Journal of*
Science, 305, 546–595, 2005.
- 775 Mauriac, R., Moutin, T., and Baklouti, M.: Accumulation of DOC in Low Phosphate Low Chlorophyll (LPLC)
area: is it related to higher production under high N:P ratio?, *Biogeosciences*, 8, 933–950, doi:10.5194/bg-
8-933-2011, 2011.
- Monteiro, F. M., Follows, M. J., and Dutkiewicz, S.: Distribution of diverse nitrogen fixers in the
global ocean: diverse nitrogen fixers in global ocean, *Global Biogeochemical Cycles*, 24, n/a–n/a,
780 doi:10.1029/2009GB003731, 2010.



- Monteiro, F. M., Dutkiewicz, S., and Follows, M. J.: Biogeographical controls on the marine nitrogen fixers: controls on marine nitrogen fixers, *Global Biogeochemical Cycles*, 25, n/a–n/a, doi:10.1029/2010GB003902, 2011.
- Moore, C. M., Mills, M. M., Langlois, R., Milne, A., Achterberg, E. P., La Roche, J., and Geider, R. J.:
785 Relative influence of nitrogen and phosphorous availability on phytoplankton physiology and productiv-
ity in the oligotrophic sub-tropical North Atlantic Ocean, *Limnology and Oceanography*, 53, 291–305,
doi:10.4319/lo.2008.53.1.0291, 2008.
- Moore, C. M., Mills, M. M., Arrigo, K. R., Berman-Frank, I., Bopp, L., Boyd, P. W., Galbraith, E. D., Geider,
R. J., Guieu, C., Jaccard, S. L., Jickells, T. D., La Roche, J., Lenton, T. M., Mahowald, N. M., Marañón, E.,
790 Marinov, I., Moore, J. K., Nakatsuka, T., Oschlies, A., Saito, M. A., Thingstad, T. F., Tsuda, A., and Ulloa, O.:
Processes and patterns of oceanic nutrient limitation, *Nature Geoscience*, 6, 701–710, doi:10.1038/ngeo1765,
2013.
- Moore, J. K., Doney, S. C., Glover, D. M., and Fung, I. Y.: Iron cycling and nutrient-limitation patterns in
surface waters of the World Ocean, *Deep Sea Research Part II: Topical Studies in Oceanography*, 49, 463–
795 507, 2001a.
- Moore, J. K., Doney, S. C., Kleypas, J. A., Glover, D. M., and Fung, I. Y.: An intermediate complexity marine
ecosystem model for the global domain, *Deep Sea Research Part II: Topical Studies in Oceanography*, 49,
403–462, 2001b.
- Moore, J. K., Doney, S. C., and Lindsay, K.: Upper ocean ecosystem dynamics and iron cycling in a global three-
800 dimensional model: global ecosystem-biogeochemical model, *Global Biogeochemical Cycles*, 18, n/a–n/a,
doi:10.1029/2004GB002220, 2004.
- Morel, A.: Optical modeling of the upper ocean in relation to its biogenous matter content (case I waters),
Journal of Geophysical Research: Oceans, 93, 10 749–10 768, doi:10.1029/JC093iC09p10749, 1988.
- Moutin, T., Van Den Broeck, N., Beker, B., Dupouy, C., Rimmelin, P., and Le Bouteiller, A.: Phosphate avail-
805 ability controls *Trichodesmium* spp. biomass in the SW Pacific Ocean, *Marine Ecology Progress Series*, 297,
15–21, 2005.
- Moutin, T., Karl, D. M., Duhamel, S., Rimmelin, P., Raimbault, P., Van Mooy, B. A. S., Claustre, H., and
others: Phosphate availability and the ultimate control of new nitrogen input by nitrogen fixation in the
tropical Pacific Ocean, *Biogeosciences Discussions*, 4, 2407–2440, 2008.
- 810 Mulholland, M. R., Bernhardt, P. W., Heil, C. A., Bronk, D. A., and O’Neil, J. M.: Nitrogen fixation and release
of fixed nitrogen by *Trichodesmium* spp. in the Gulf of Mexico, *Limnology and Oceanography*, 51, 1762–
1776, 2006.
- O’Neil, J. and Roman, M.: *Marine Pelagic Cyanobacteria: Trichodesmium and other Diazotrophs. Grazers and
associated organisms of Trichodesmium*, Springer Netherlands, 1992.
- 815 O’Neil, J. M., Metzler, P. M., and Glibert, P. M.: Ingestion of ¹⁵N₂-labelled *Trichodesmium* spp. and am-
monium regeneration by the harpacticoid copepod *Macrosetella gracilis*, *Marine Biology*, 125, 89–96,
doi:10.1007/BF00350763, 1996.
- Ouillon, S., Douillet, P., Lefebvre, J., Le Gendre, R., Jouon, A., Bonneton, P., Fernandez, J., Chevil-
lon, C., Magand, O., Lefèvre, J., Le Hir, P., Laganier, R., Dumas, F., Marchesiello, P., Bel Madani,
820 A., Andréfouët, S., Panché, J., and Fichez, R.: Circulation and suspended sediment transport in a



- coral reef lagoon: The south-west lagoon of New Caledonia, *Marine Pollution Bulletin*, 61, 269–296, doi:10.1016/j.marpolbul.2010.06.023, 2010.
- Pakulski, J. D. and Benner, R.: Abundance and distribution of carbohydrates in the ocean, *Limnology and Oceanography*, 39, 930–940, doi:10.4319/lo.1994.39.4.0930, 1994.
- 825 Rabouille, S., Staal, M., Stal, L. J., and Soetaert, K.: Modeling the Dynamic Regulation of Nitrogen Fixation in the Cyanobacterium *Trichodesmium* sp., *Applied and Environmental Microbiology*, 72, 3217–3227, doi:10.1128/AEM.72.5.3217-3227.2006, 2006.
- Raimbault, P. and Garcia, N.: Evidence for efficient regenerated production and dinitrogen fixation in nitrogen-deficient waters of the South Pacific Ocean: impact on new and export production estimates, *Biogeosciences*, 5, 323–338, 2008.
- 830 Reddy, K. J., Haskell, J. B., Sherman, D. M., and Sherman, L. A.: Unicellular, aerobic nitrogen-fixing cyanobacteria of the genus *Cyanothece*, *Journal of Bacteriology*, 175, 1284–1292, 1993.
- Rodier, M. and Le Borgne, R.: Population dynamics and environmental conditions affecting *Trichodesmium* spp. (filamentous cyanobacteria) blooms in the south–west lagoon of New Caledonia, *Journal of Experimental Marine Biology and Ecology*, 358, 20–32, 2008.
- 835 Rodier, M. and Le Borgne, R.: Population and trophic dynamics of *Trichodesmium thiebautii* in the SE lagoon of New Caledonia. Comparison with *T. erythraeum* in the SW lagoon, *Marine Pollution Bulletin*, 61, 349–359, doi:10.1016/j.marpolbul.2010.06.018, 2010.
- Roenneberg, T. and Carpenter, E. J.: Daily rhythm of O₂-evolution in the cyanobacterium *Trichodesmium thiebautii* under natural and constant conditions, *Marine Biology*, 117, 693–697, doi:10.1007/BF00349782, 1993.
- 840 Sohm, J. A., Edwards, B. R., Wilson, B. G., and Webb, E. A.: Constitutive Extracellular Polysaccharide (EPS) Production by Specific Isolates of *Crocospaera watsonii*, *Frontiers in Microbiology*, 2, doi:10.3389/fmicb.2011.00229, 2011.
- 845 Subramaniam, A., Yager, P. L., Carpenter, E. J., Mahaffey, C., Björkman, K., Cooley, S., Kustka, A. B., Montoya, J. P., Sañudo-Wilhelmy, S. A., Shipe, R., and Capone, D. G.: Amazon River enhances diazotrophy and carbon sequestration in the tropical North Atlantic Ocean, *Proceedings of the National Academy of Sciences*, 105, 10 460–10 465, doi:10.1073/pnas.0710279105, 2008.
- Tanaka, T., Thingstad, T. F., Christaki, U., Colombet, J., Cornet-Barthaux, V., Courties, C., Grattepanche, J.-D., Lagaria, A., Nedoma, J., Oriol, L., Psarra, S., Pujo-Pay, M., and Van Wambeke, F.: Lack of P-limitation of phytoplankton and heterotrophic prokaryotes in surface waters of three anticyclonic eddies in the stratified Mediterranean Sea, *Biogeosciences*, 8, 525–538, doi:10.5194/bg-8-525-2011, 2011.
- 850 Thingstad, T. F., Krom, M. D., Mantoura, R. F. C., Flaten, G. F., Groom, S., Herut, B., Kress, N., Law, C. S., Pasternak, A., Pitta, P., and others: Nature of phosphorus limitation in the ultraoligotrophic eastern Mediterranean, *Science*, 309, 1068–1071, 2005.
- 855 Turk-Kubo, K., Frank, I., Hogan, M., Desnues, A., Bonnet, S., and Zehr, J. P.: Diazotroph community succession during the VAHINE mesocosms experiment (New Caledonia Lagoon), *Biogeosciences*, subm.
- Van Wambeke, F., Preunfdt, U., Barani, A., Berthelot, H., Moutin, T., Rodier, M., Hess, W., and Bonnet, S.: Heterotrophic bacterial production and metabolic balance during the VAHINE mesocosm experiment in the New Caledonia lagoon, *Biogeosciences*, subm.
- 860



- Van Wambeke, F., Bonnet, S., Moutin, T., Raimbault, P., Alarcón, G., Guieu, C., and others: Factors limiting heterotrophic bacterial production in the southern Pacific Ocean, *Biogeosciences*, 5, 833–845, 2008.
- Villareal, T. A., Woods, S., Moore, J. K., and CulverRymysza, K.: Vertical migration of *Rhizosolenia* mats and their significance to NO₃⁻ fluxes in the central North Pacific gyre, *Journal of Plankton Research*, 18, 1103–1121, 1996.
- 865 Zohary, T., Herut, B., Krom, M. D., Fauzi C. Mantoura, R., Pitta, P., Psarra, S., Rassoulzadegan, F., Stambler, N., Tanaka, T., Frede Thingstad, T., and Malcolm S. Woodward, E.: P-limited bacteria but N and P co-limited phytoplankton in the Eastern Mediterranean—a microcosm experiment, *Deep Sea Research Part II: Topical Studies in Oceanography*, 52, 3011–3023, doi:10.1016/j.dsr2.2005.08.011, 2005.



870 List of Figures

- 1 Conceptual diagram of the biogeochemical model for the 1D-vertical model used in
the VAHINE experiment. 31
- 2 Conceptual diagram of the DDN pathway with compartments and processes engaged
in the DDN transfer within the food web. 32
- 875 3 Temporal evolution of (a) dissolved inorganic phosphate (DIP), (b) nitrate (NO_3^-),
(c) dissolved organic phosphate (DOP), (d) dissolved organic nitrogen (DON), (e)
particulate organic phosphorus (POP), (f) particulate organic nitrogen (PON), (g)
total phosphorus (P_{total}) and (h) total nitrogen (N_{total}) concentrations ($\mu\text{mol.L}^{-1}$)
in model outputs (solid lines : SIM^E (blue) and SIM^C (black)) averaged on depth
880 superposed to data observations averaged on depth in the three mesocosms (M1
(red), M2 (blue), M3 (green)) and in surrounding waters (black). Red vertical lines
distinguish the three periods P0 (before the DIP enrichment), P1 (Diatom-diazotroph
associations dominate the diazotrophic community) and P2 (unicellular N_2 -fixing
cyanobacteria (Group C) dominate the diazotrophic community). 33
- 885 4 Temporal evolution of (a) dinitrogen fixation (N_2 fixation) rates ($\text{nmolN.L}^{-1}.\text{d}^{-1}$)
, (b) dissolved inorganic phosphate turnover time (T_{DIP} , days) , (c) chlorophyll a
(Chl a, $\mu\text{g.L}^{-1}$), (d) particulate organic C exported (POC_{exp} , dry matter in mmolC
, (e) primary production (PP) rates ($\mu\text{molC.L}^{-1}.\text{d}^{-1}$), (f) particulate organic ni-
trogen exported * 16 (PON_{exp} , dry matter in mmolN), (g) Bacterial production
890 (BP) rates ($\mu\text{molC.L}^{-1}.\text{d}^{-1}$) and (h) particulate organic phosphate exported * 106
(POP_{exp} , dry matter in mmolN) in model outputs (solid lines : SIM^E (blue) and
 SIM^C (black)) averaged on depth superposed to data observations averaged on depth
in the three mesocosms (M1 (red), M2 (blue), M3 (green)) and in surrounding waters
(black). Red vertical lines distinguish the three periods P0 (before the DIP enrich-
895 ment), P1 (Diatom-diazotroph associations dominate the diazotrophic community)
and P2 (unicellular N_2 -fixing cyanobacteria (Group C) dominate the diazotrophic
community). 34



- 5 Abundances temporal evolution of (a) *Trichodesmium* (TRI, trichom.L⁻¹), (b) uni-
cellular N₂-fixing cyanobacteria (UCYN-C, cell.L⁻¹), (c) large phytoplankton (PHYL,
900 cell.L⁻¹), (d) small phytoplankton (PHYS, cell.L⁻¹), (e) heterotrophic bacteria (BAC,
cell.L⁻¹), (f) hetero-nanoflagellates (HNF, ind.L⁻¹), ciliates (CIL, ind.L⁻¹) and
copepods (COP, ind.L⁻¹) in model outputs (solid lines : SIM^E (blue) and SIM^C
(black)) averaged on depth superposed to data observations averaged on depth in
the three mesocosms (M1 (red), M2 (blue), M3 (green)) and in surrounding waters
905 (black). Red vertical lines distinguish the three periods P0 (before the DIP enrich-
ment), P1 (Diatom-diazotroph associations dominate the diazotrophic community)
and P2 (unicellular N₂-fixing cyanobacteria (Group C) dominate the diazotrophic
community). 35
- 6 Temporal evolution of specific- (green) and population (blue) growth rates func-
910 tion of (a) unicellular N₂-fixing cyanobacteria (UCYN-C, cell.s⁻¹) and (b) *Tri-
chodesmium* (TRI, trichome.s⁻¹) and carbon (C, blue), nitrogen (N, green) and
phosphorus (P, red) relative intracellular quota in (c) unicellular N₂-fixing cyanobac-
teria (Group C) (UCYN-C, %) and (d) *Trichodesmium* (TRI, %) in model outputs
in SIM^E. Red vertical lines distinguish the three periods P0 (before the DIP enrich-
915 ment), P1 (Diatom-diazotroph associations dominate the diazotrophic community)
and P2 (unicellular N₂-fixing cyanobacteria (Group C) dominate the diazotrophic
community). 36
- 7 Temporal evolution of DDN proportion (%) in (a) *Trichodesmium* (TRI), (b) uni-
cellular N₂-fixing cyanobacteria (Group C) (UCYN-C), (c) dissolved organic nitro-
920 gen (DON), (d) ammonium (NH₄⁺), (e) nitrate (NO₃⁻) (f) detrital nitrogen (DET_N),
(g) heterotrophic bacteria (BAC), (h) small phytoplankton (PHYS), (i) large phyto-
plankton (PHYL), (j) hetero-nanoflagellates (HNF), (k) ciliates (CIL), (l) copepods
(COP) and (m) in traps (TRAP) in SIM^E. Red vertical lines distinguish the three pe-
riods P0 (before the DIP enrichment), P1 (Diatom-diazotroph associations dominate
925 the diazotrophic community) and P2 (unicellular N₂-fixing cyanobacteria (Group C)
dominate the diazotrophic community). 37
- 8 Temporal evolution of the nitrogen fixation contribution (%) to particulate matter
export in SIM^E. 38

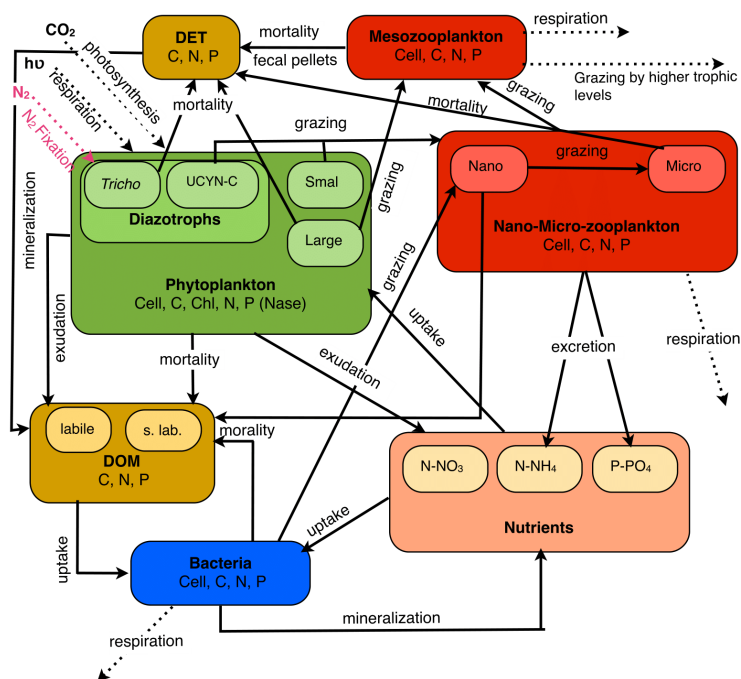


Figure 1. Conceptual diagram of the biogeochemical model for the 1D-vertical model used in the VAHINE experiment.

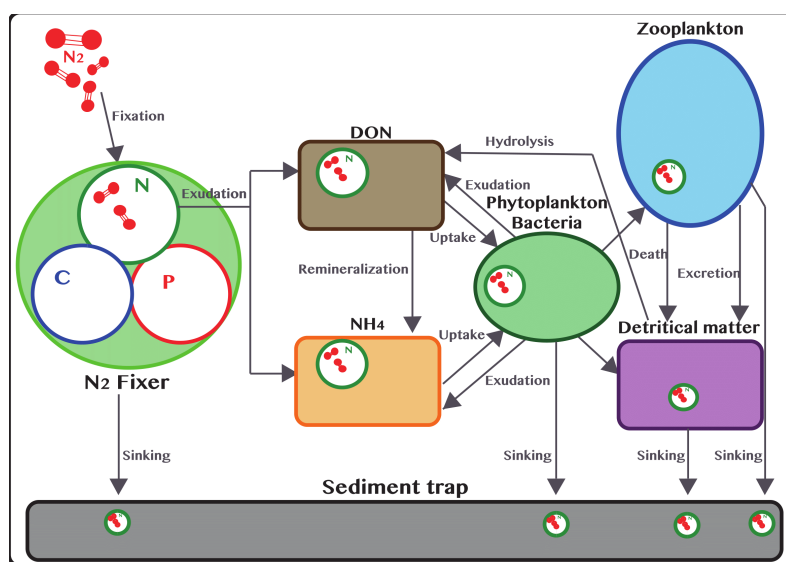


Figure 2. Conceptual diagram of the DDN pathway with compartments and processes engaged in the DDN transfer within the food web.

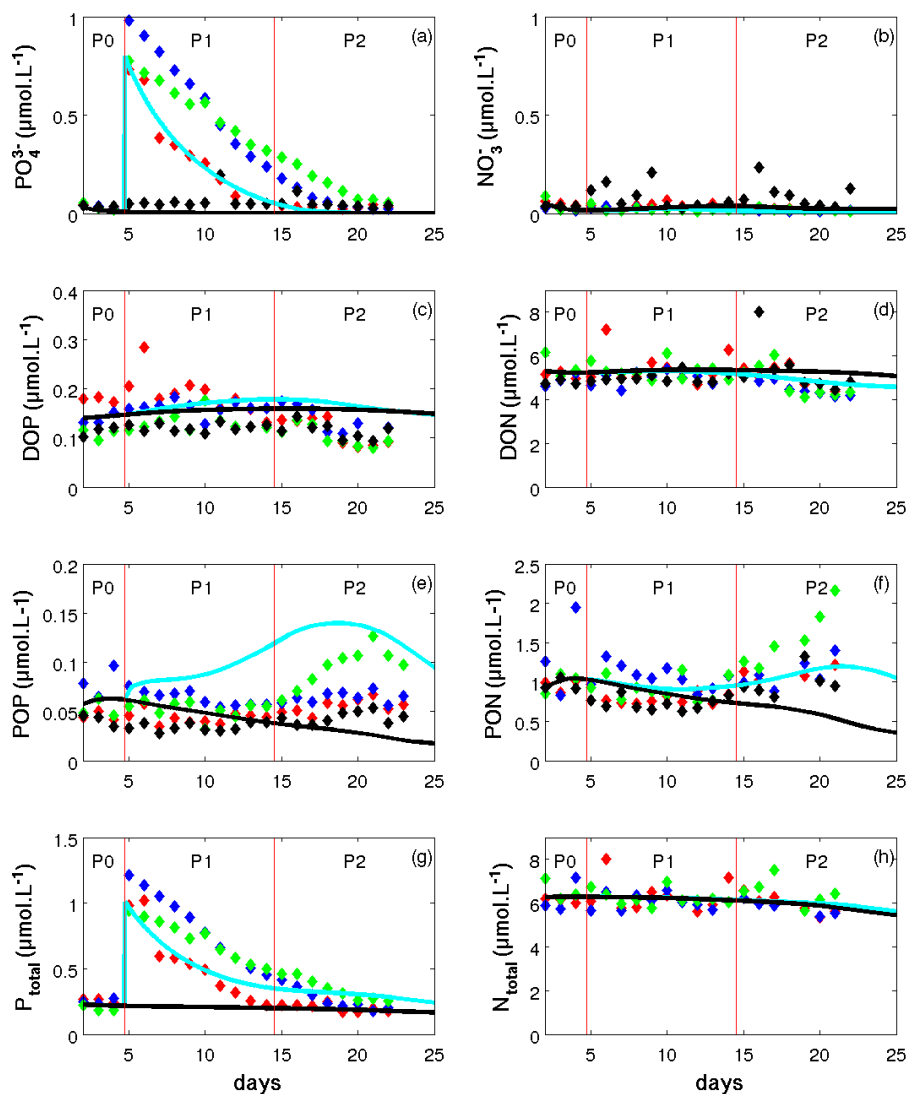


Figure 3. Temporal evolution of (a) dissolved inorganic phosphate (DIP), (b) nitrate (NO_3^-), (c) dissolved organic phosphate (DOP), (d) dissolved organic nitrogen (DON), (e) particulate organic phosphorus (POP), (f) particulate organic nitrogen (PON), (g) total phosphorus (P_{total}) and (h) total nitrogen (N_{total}) concentrations ($\mu\text{mol.L}^{-1}$) in model outputs (solid lines : SIM^E (blue) and SIM^C (black)) averaged on depth superposed to data observations averaged on depth in the three mesocosms (M1 (red), M2 (blue), M3 (green)) and in surrounding waters (black). Red vertical lines distinguish the three periods P0 (before the DIP enrichment), P1 (Diatom-diazotroph associations dominate the diazotrophic community) and P2 (unicellular N_2 -fixing cyanobacteria (Group C) dominate the diazotrophic community).

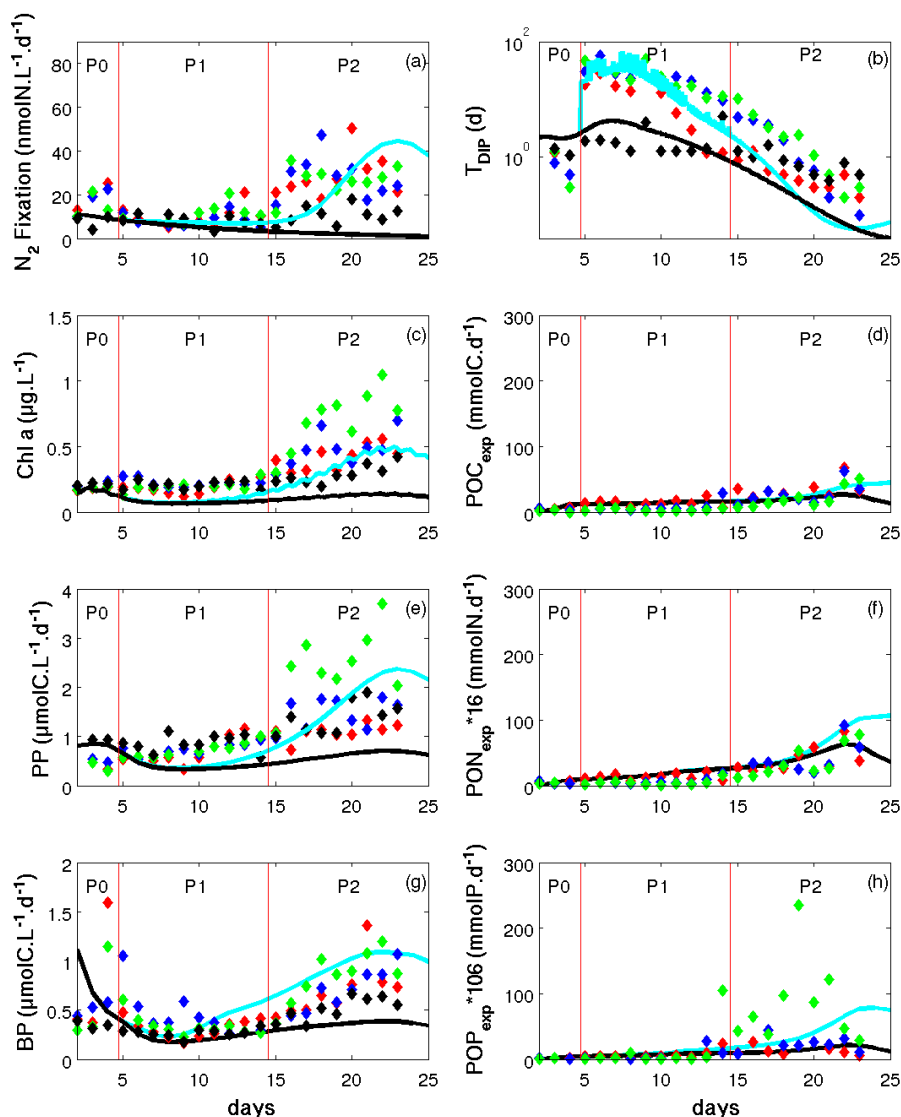


Figure 4. Temporal evolution of (a) dinitrogen fixation (N_2 fixation) rates ($\text{nmolN.L}^{-1}.\text{d}^{-1}$), (b) dissolved inorganic phosphate turnover time (T_{DIP} , days), (c) chlorophyll a (Chl a, $\mu\text{g.L}^{-1}$), (d) particulate organic C exported (POC_{exp} , dry matter in mmolC), (e) primary production (PP) rates ($\mu\text{molC.L}^{-1}.\text{d}^{-1}$), (f) particulate organic nitrogen exported * 16 (PON_{exp} , dry matter in mmolN), (g) Bacterial production (BP) rates ($\mu\text{molC.L}^{-1}.\text{d}^{-1}$) and (h) particulate organic phosphate exported * 106 (POP_{exp} , dry matter in mmolN) in model outputs (solid lines: SIM^E (blue) and SIM^C (black)) averaged on depth superposed to data observations averaged on depth in the three mesocosms (M1 (red), M2 (blue), M3 (green)) and in surrounding waters (black).

Red vertical lines distinguish the three periods P0 (before the DIP enrichment), P1 (Diatom-diazotroph associations dominate the diazotrophic community) and P2 (unicellular N_2 -fixing cyanobacteria (Group C) dominate the diazotrophic community).

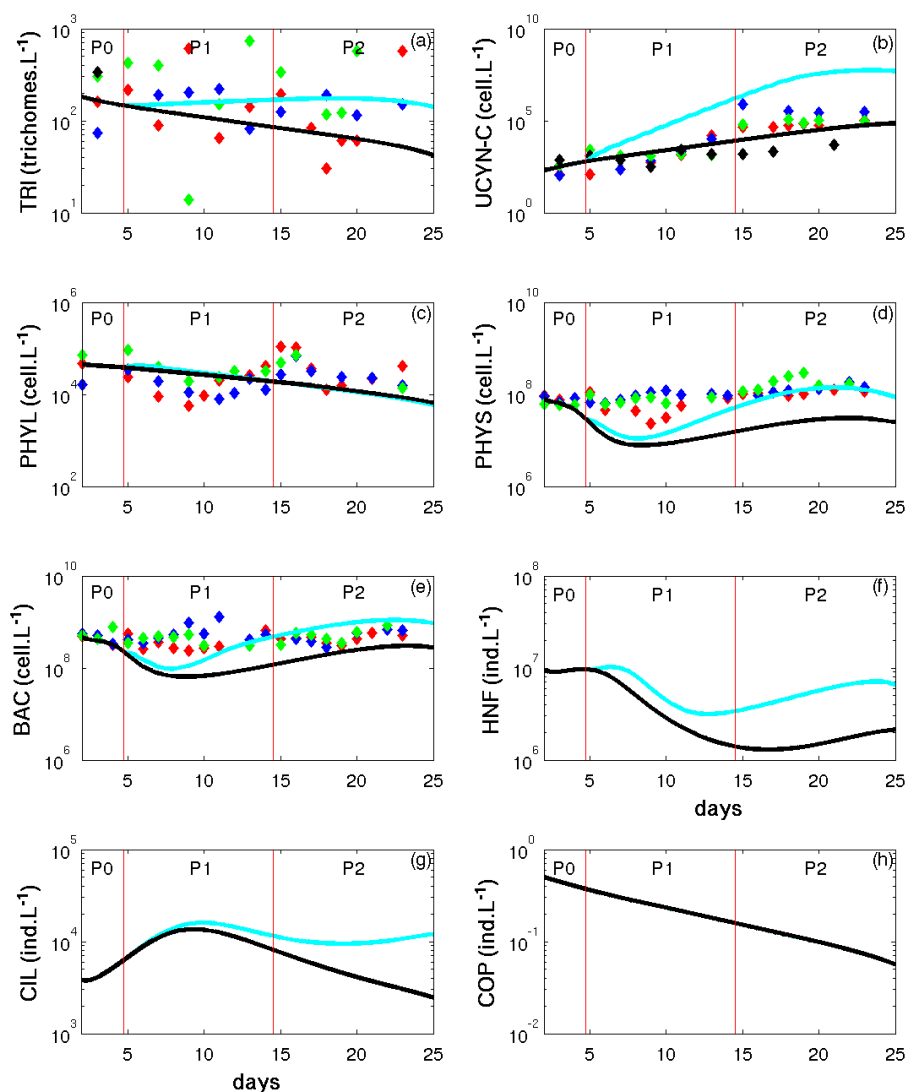


Figure 5. Abundances temporal evolution of (a) *Trichodesmium* (TRI, trichom.L⁻¹), (b) unicellular N₂-fixing cyanobacteria (UCYN-C, cell.L⁻¹), (c) large phytoplankton (PHYL, cell.L⁻¹), (d) small phytoplankton (PHYS, cell.L⁻¹), (e) heterotrophic bacteria (BAC, cell.L⁻¹), (f) hetero-nanoflagellates (HNF, ind.L⁻¹), ciliates (CIL, ind.L⁻¹) and copepods (COP, ind.L⁻¹) in model outputs (solid lines : SIM^E (blue) and SIM^C (black)) averaged on depth superposed to data observations averaged on depth in the three mesocosms (M1 (red), M2 (blue), M3 (green)) and in surrounding waters (black). Red vertical lines distinguish the three periods P0 (before the DIP enrichment), P1 (Diatom-diazotroph associations dominate the diazotrophic community) and P2 (unicellular N₂-fixing cyanobacteria (Group C) dominate the diazotrophic community).

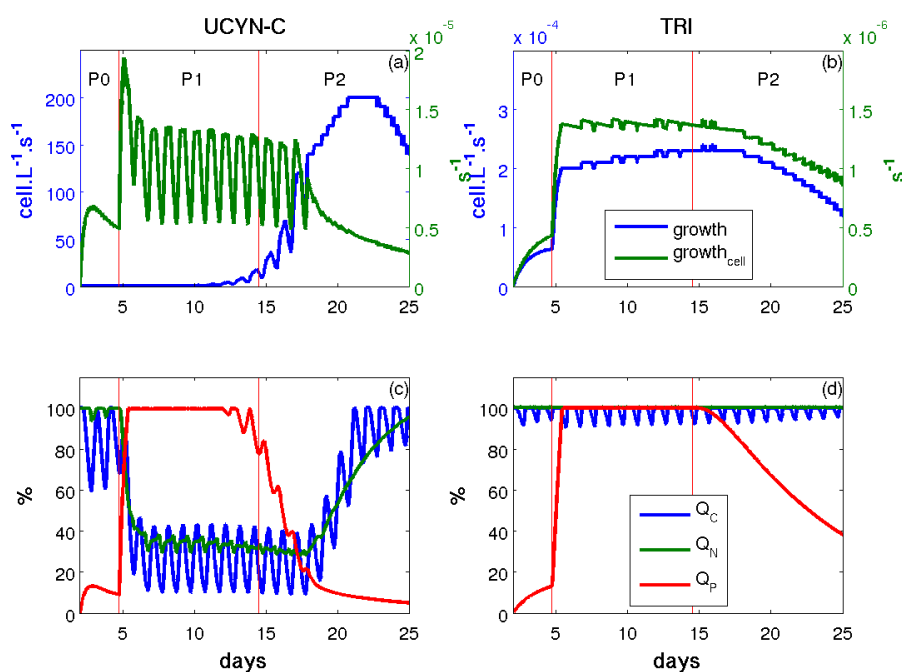


Figure 6. Temporal evolution of specific- (green) and population (blue) growth rates function of (a) unicellular N_2 -fixing cyanobacteria (UCYN-C, cell.s^{-1}) and (b) *Trichodesmium* (TRI, trichome.s^{-1}) and carbon (C, blue), nitrogen (N, green) and phosphorus (P, red) relative intracellular quota in (c) unicellular N_2 -fixing cyanobacteria (Group C) (UCYN-C, %) and (d) *Trichodesmium* (TRI, %) in model outputs in SIM^E. Red vertical lines distinguish the three periods P0 (before the DIP enrichment), P1 (Diatom-diazotroph associations dominate the diazotrophic community) and P2 (unicellular N_2 -fixing cyanobacteria (Group C) dominate the diazotrophic community).

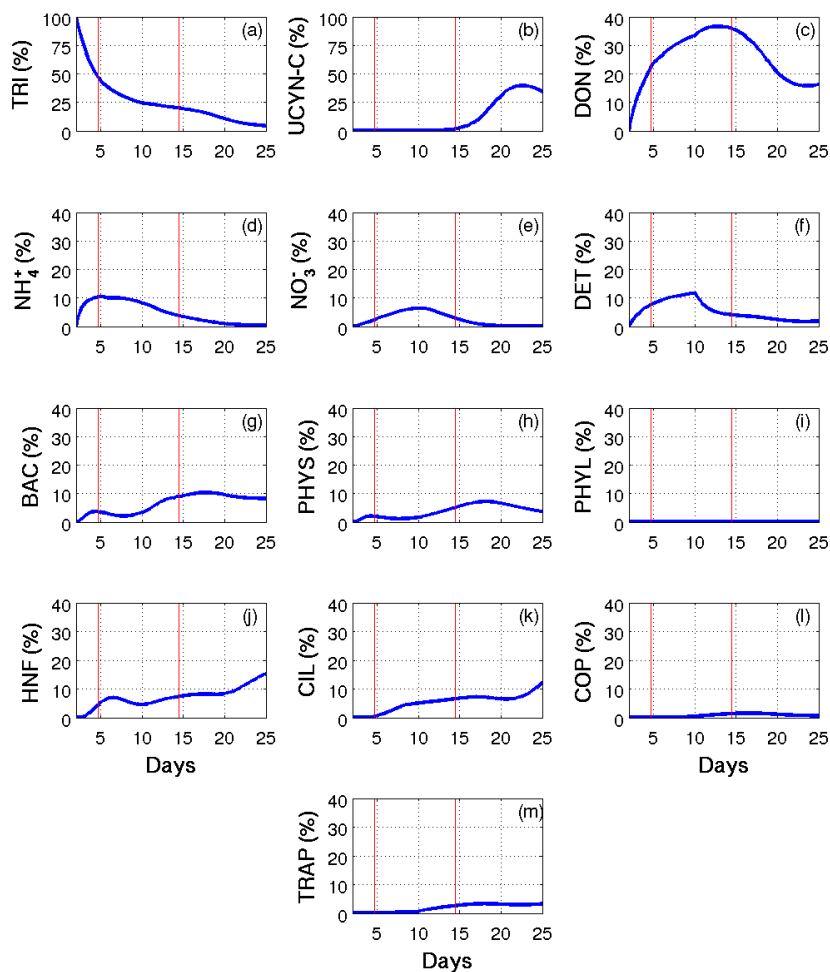


Figure 7. Temporal evolution of DDN proportion (%) in (a) *Trichodesmium* (TRI), (b) unicellular N_2 -fixing cyanobacteria (Group C) (UCYN-C), (c) dissolved organic nitrogen (DON), (d) ammonium (NH_4^+), (e) nitrate (NO_3^-) (f) detrital nitrogen (DET_N), (g) heterotrophic bacteria (BAC), (h) small phytoplankton (PHYS), (i) large phytoplankton (PHYL), (j) hetero-nanoflagellates (HNF), (k) ciliates (CIL), (l) copepods (COP) and (m) in traps (TRAP) in SIM^E . Red vertical lines distinguish the three periods P0 (before the DIP enrichment), P1 (Diatom-diazotroph associations dominate the diazotrophic community) and P2 (unicellular N_2 -fixing cyanobacteria (Group C) dominate the diazotrophic community)

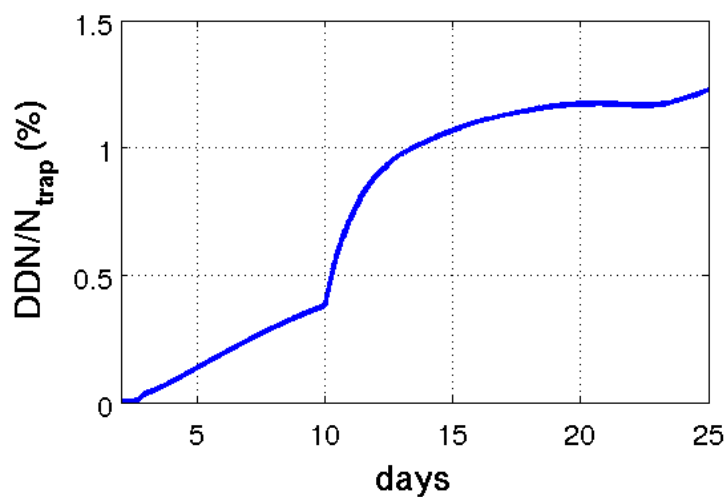


Figure 8. Temporal evolution of the nitrogen fixation contribution (%) to particulate matter export in SIM^E.



State variable	Reference	Value	Unit	State variable	Reference	Value	Unit
BAC_{cell}	Data	$4.75 \cdot 10^8$	$cell.L^{-1}$	HNF_{cell}	$\frac{BAC_{cell}}{50}$	$9.519 \cdot 10^6$	$ind.L^{-1}$
BAC_C	$BAC_{cell} \times Q_C^{max}$	1.152	$\mu mol C.L^{-1}$	HNF_C	$HNF_{cell} \times Q_C^{max}$	34.950	$\mu mol C.L^{-1}$
BAC_N	$BAC_{cell} \times Q_N^{moy} \times 0.7$	0.107	$\mu mol N.L^{-1}$	HNF_N	$HNF_{cell} \times Q_N^{moy} \times 0.7$	0.326	$\mu mol N.L^{-1}$
BAC_P	$BAC_{cell} \times Q_P^{min}$	0.007	$\mu mol P.L^{-1}$	HNF_P	$HNF_{cell} \times Q_P^{min}$	0.023	$mol P.L^{-1}$
CIL_{cell}	$\frac{HNF_{cell}}{2500}$	3808	$ind.L^{-1}$	$MZOO_{cell}$	Adapted data	0.5	$ind.L^{-1}$
CIL_C	$CIL_{cell} \times Q_C^{max}$	1.538	$\mu mol C.L^{-1}$	$MZOO_C$	$MZOO_{cell} \times Q_C^{max}$	0.350	$\mu mol C.L^{-1}$
CIL_N	$CIL_{cell} \times Q_N^{moy} \times 0.7$	0.108	$\mu mol N.L^{-1}$	$MZOO_N$	$MZOO_{cell} \times Q_N^{moy} \times 0.7$	0.042	$\mu mol N.L^{-1}$
CIL_P	$CIL_{cell} \times Q_P^{min}$	0.005	$\mu mol P.L^{-1}$	$MZOO_P$	$MZOO_{cell} \times Q_P^{min}$	0.002	$\mu mol P.L^{-1}$
$PHYL_{cell}$	Data	$4.48 \cdot 10^4$	$cell.L^{-1}$	$PHYS_{cell}$	Data	$8.11 \cdot 10^7$	$cell.L^{-1}$
$PHYL_C$	$PHYL_{cell} \times Q_C^{max}$	0.306	$\mu mol C.L^{-1}$	$PHYS_C$	$PHYS_{cell} \times Q_C^{max}$	1.664	$\mu mol C.L^{-1}$
$PHYL_N$	$PHYL_{cell} \times Q_N^{moy} \times 0.7$	0.022	$\mu mol N.L^{-1}$	$PHYS_N$	$PHYS_{cell} \times Q_N^{moy} \times 0.7$	0.117	$\mu mol N.L^{-1}$
$PHYL_P$	$PHYL_{cell} \times Q_P^{min}$	$9.634 \cdot 10^{-4}$	$mol P.L^{-1}$	$PHYS_P$	$PHYS_{cell} \times Q_P^{min}$	0.005	$\mu mol P.L^{-1}$
$PHYL_{Chl}$	$\frac{PHYL_C}{25}$	0.012	$\mu g Chl.L^{-1}$	$PHYS_{Chl}$	$\frac{PHYS_C}{12}$	0.138	$\mu g Chl.L^{-1}$
$UCYN - C_{cell}$	Data	210	$cell.L^{-1}$	TRI_{cell}	Data	180	$cell.L^{-1}$
$UCYN - C_C$	$UCYN - C_{cell} \times Q_C^{max}$	4.308	$pmol C.L^{-1}$	TRI_C	$TRI_{cell} \times Q_C^{max}$		$mol C.L^{-1}$
$UCYN - C_N$	$UCYN - C_{cell} \times Q_N^{max}$	0.650	$pmol N.L^{-1}$	TRI_N	$TRI_{cell} \times Q_N^{max}$		$mol N.L^{-1}$
$UCYN - C_P$	$UCYN - C_{cell} \times Q_P^{min}$	0.013	$pmol P.L^{-1}$	TRI_P	$TRI_{cell} \times Q_P^{min}$		$mol P.L^{-1}$
$UCYN - C_{Nase}$	$\frac{TRI_{Nase}}{33300}$	$1.9 \cdot 10^{20}$	$mol N.cell^{-1}.s^{-1}$	$TRONase$	Rabouille et al. 2006	$7.5 \cdot 10^{16}$	$mol N.trich^{-1}.s^{-1}$
$UCYN - C_{Chl}$	$\frac{UCYN - C_C}{12}$	0.359	$pg Chl.L^{-1}$	TRI_{Chl}	$\frac{TRI_C}{25}$		$g Chl.L^{-1}$
labile DOC	Data	0.25	$\mu mol C.L^{-1}$	POC_{Det}	$POC_{Tot} - POC_{Living}$		$\mu mol C.L^{-1}$
semi labile DOC	labile DOC $\times 19$	4.75	$\mu mol C.L^{-1}$	PON_{Det}	$PON_{Tot} - PON_{Living}$		$\mu mol N.L^{-1}$
labile DON	Data	1.0	$\mu mol N.L^{-1}$	POP_{Det}	$POP_{Tot} - POP_{Living}$		$\mu mol P.L^{-1}$
labile DOP	Data	0.0132	$\mu mol P.L^{-1}$				
NO_3^-	Data	53	$nmol L^{-1}$				
NH_4	Data	36	$nmol L^{-1}$				
PO_4	Data	30	$nmol L^{-1}$				

Table 1. Initial conditions for the biogeochemical model



Parameter	Definition	TRI value	UCYN-C value	unit
Q_C^{min}	minimum quota of C	$2.28 \cdot 10^{-10}$	$6.84 \cdot 10^{-15}$	$molC.Cell^{-1}$
Q_C^{max}	maximum quota of C	$6.84 \cdot 10^{-15}$	$2.05 \cdot 10^{-14}$	$molC.Cell^{-1}$
Q_N^{min}	minimum quota of N	$3.44 \cdot 10^{-11}$	$1.03 \cdot 10^{-15}$	$molN.Cell^{-1}$
Q_N^{max}	maximum quota of N	$1.03 \cdot 10^{-10}$	$3.09 \cdot 10^{-15}$	$molN.Cell^{-1}$
Q_P^{min}	minimum quota of P	$3.44 \cdot 10^{-11}$	$1.03 \cdot 10^{-15}$	$molN.Cell^{-1}$
Q_P^{max}	maximum quota of P	$1.03 \cdot 10^{-10}$	$3.09 \cdot 10^{-15}$	$molN.Cell^{-1}$
Q_{CN}^{min}	minimum C:N ratio	5.0	5.0	$molC.molN^{-1}$
Q_{CN}^{max}	maximum C:N ratio	19.8	19.8	$molC.molN^{-1}$
Q_{CP}^{min}	minimum C:P ratio	35.33	35.33	$molC.molP^{-1}$
Q_{CP}^{max}	maximum C:P ratio	318.0	318.0	$molC.molP^{-1}$
μ_{max}	maximum growth rate	$2.08 \cdot 10^{-6}$	$3.2 \cdot 10^{-5}$	s^{-1}
k_m	specific natural mortality rate	$1.16 \cdot 10^{-6}$	$1.16 \cdot 10^{-6}$	s^{-1}
K_{NO^3}	Half-saturation constant for NO^3	$1.85 \cdot 10^{-6}$	$7.6 \cdot 10^{-6}$	$mol.L^{-1}$
$V_{NO^3}^{max}$	Maximum uptake rate for NO^3	$3.16 \cdot 10^{-15}$	$9.91 \cdot 10^{-20}$	$mol.cell^{-1}.s^{-1}$
K_{NH^4}	Half-saturation constant for NH^4	$7.0 \cdot 10^{-6}$	$1.69 \cdot 10^{-6}$	$mol.L^{-1}$
$V_{NH^4}^{max}$	Maximum uptake rate for NH^4	$3.16 \cdot 10^{-15}$	$9.91 \cdot 10^{-20}$	$mol.cell^{-1}.s^{-1}$
K_{PO^4}	Half-saturation constant for PO^4	$1.4 \cdot 10^{-6}$	$2.62 \cdot 10^{-7}$	$mol.L^{-1}$
$V_{PO^4}^{max}$	Maximum uptake rate for PO^4	$1.98 \cdot 10^{-16}$	$6.19 \cdot 10^{-21}$	$mol.cell^{-1}.s^{-1}$
K_{DON}	Half-saturation constant for DON	$4.32 \cdot 10^{-5}$	$1.05 \cdot 10^{-5}$	$mol.L^{-1}$
V_{DON}^{max}	Maximum uptake rate for DON	$3.16 \cdot 10^{-15}$	$9.91 \cdot 10^{-20}$	$mol.cell^{-1}.s^{-1}$
K_{DOP}	Half-saturation constant for DOP	$3.4 \cdot 10^{-6}$	$6.57 \cdot 10^{-7}$	$mol.L^{-1}$
V_{DOP}^{max}	Maximum uptake rate for DOP	$3.16 \cdot 10^{-15}$	$6.19 \cdot 10^{-21}$	$mol.cell^{-1}.s^{-1}$
$Nase_{prod}^{max}$	Maximum rate of increase of nitrogenase activity	$1.17 \cdot 10^{-21}$	$3.51 \cdot 10^{-26}$	$mol.cell^{-1}.s^{-2}$
$Nase_{decr}^{max}$	Maximum rate of decay of nitrogenase activity	$9.36 \cdot 10^{-22}$	$2.83 \cdot 10^{-26}$	$mol.cell^{-1}.s^{-2}$
K_{Nase}	Coefficient of nitrogenase degradation	$9.44 \cdot 10^{-16}$	$1.92 \cdot 10^{-20}$	$mol.cell^{-1}.s^{-1}$
$COST_{DIAZO}$	Respiration cost for nitrogen fixation	1.5	1.5	$mol.mol^{-1}$
$EXUD_{DON}$	Exsudation part of N_2 fixed towards DON	0.5	0.5	
$EXUD_{NH_4}$	Exsudation part of N_2 fixed towards NH_4	0.5	0.5	

Table 2. Parameters added for the diazotroph organisms